ESA Contract No. 4000130930/20/I-DT

TOWARDS THE RETRIEVAL OF LAKE ICE THICKNESS FROM SATELLITE ALTIMETRY MISSIONS

(LIAM)

Mid-Term Review Report

Issue / Revision: 1 / 2

Date: 27.03.2021

Prepared by

Claude Duguay, H2O Geomatics Inc. Justin Murfitt, University of Waterloo
Ghislain Picard, Institut des Géosciences de l'Environnement-Université Grenoble Alpes
Elena Zakharova, Ocean Next (now with EOLA Micro-Enterprise)

APPROVAL

Signature		
Date	27.03.2021	2021.03.29
Surname	C. Duguay	J. Benveniste
Affiliation	H2O Geomatics	ESA

ESA STUDY CONTRACT REPORT

ESA CONTRACT NO.	SUBJECT:	CONTRACTOR:
4000130930/20/I-DT	LIAM – Mid-Term Review Report	H2O Geomatics Inc.

ABSTRACT:

This Mid-Term Review Report contains a description of the outcomes of activities carried out under WP 200 (Forward modelling of backscatter and brightness temperature using the SMRT model) and WP 310 (Analysis of altimetry and radiometer data over lakes). It adds to the previously delivered Scientific and Technical Report that described findings from activities performed under WP 100 (State-of-the-art review, analysis and requirement review). Together they cover advances made over the first six months of the LIAM project.

Activities under WP 200 first involved adaptation of the Snow Microwave Radiative Transfer (SMRT) model to simulate backscatter and brightness temperature from frozen lakes with various scenarios of ice and overlying snow properties. Simulations allowed for examination of the relation between ice thickness and microwave signals as well as identification of the influence of varied ice (snow ice, bubbles, roughness at ice-water interface) and snow (depth, wetness) properties on this relation, which could be considered as potential sources of uncertainty in ice thickness retrievals from altimeter missions. The findings are described in Section 2 along with preliminary simulations of waveforms (low resolution mode) with a new altimetry module recently added to SMRT, and how coupling has now been achieved between the Canadian Lake Ice Model (CLIMo) and SMRT.

Under WP 310, several questions were investigated from altimetric and radiometric observations, specifically in relation to lake ice cover and its properties. Accordingly, Section 3 provides a detailed analysis of: 1) the impact of land contamination on measurements of radar backscatter and brightness temperature; 2) the impact of snow on-ice; 3) the impact of ice structure; 4) inter-comparison of radar and radiometer measurements of two missions – Jason and Sentinel-3; and 5) the spatio-temporal variability of Jason-2 waveforms.

Finally, key findings from the above activities are summarized in Section 4 along with a brief description of the next steps envisioned until the end of this 12-month study and findings to be included in the final report.

AUTHORS: Claude Duguay, Ghislain Picard and Elena Zakharova

ESA Study Manager: Jérôme Benveniste	ESA BUDGET HEADING

DOCUMENT CHANGE LOG

Issue/ Revision	Date	Modification	Modified pages	Comment
1/1	25.03.2021			All changes included in this version of the report are documented in file Review_LIAM_MTR_Issue_1.0_reply.docx
1/2	27.03.2021			All changes included in this version of the report are documented in file Review_LIAM_MTR_Issue_1.1_reply.docx

List of Acronyms

AMSR-E/2	Advanced Microwave Scanning Radiometer for EOS and follow-up 2
CLIMo	Canadian Lake Ice Model
CoReH2O	Cold Regions Hydrology High-resolution Observatory
ESA	European Space Agency
IBA	Improved Born Approximation
IEM	Integral Equation Model
LIAM	Lake Ice from Altimetry Missions
MODIS	Moderate Resolution Imaging Spectroradiometer
OCOG	Offset Centre of Gravity
RMS	Root mean square (height)
RMSE	Root mean square error
SAR	Synthetic aperture radar
SMRT	Snow Microwave Radiative Transfer model
Tb	Brightness temperature
UTM	Universal Transverse Mercator
WF	Waveform

Table of Contents

1. INTRODUCTION

1.1 Purpose of the document

This document contains a description of the outcomes of activities carried out under WP 200 (Forward modelling of backscatter and brightness temperature using the SMRT model) and WP 310 (Analysis of altimetry and radiometer data over lakes). It adds to the previously delivered Scientific and Technical Report which described activities under WP 100 (State-of-the-art review, analysis and requirement review). Together they cover advances made over the first six months of the LIAM project.

1.2 Structure of the document

This document contains three main sections in addition to the Introduction and list of references. Section 2 provides of description of the progress achieved under WP 200, starting first with the adaptation of the Snow Microwave Radiative Transfer (SMRT) model to simulate backscatter and brightness temperature from frozen lakes of various possible ice and snow properties. This section also covers results from preliminary simulations of waveforms with a new altimetry module recently added to SMRT and a brief description of the coupling of the Canadian Lake Ice Model (CLIMo) – a 1-D thermodynamic freshwater ice model – and SMRT. Section 3 describes progress made under WP 310. More specifically, the section contains a detailed analysis of 1) the impact of land contamination on measurements of radar backscatter and brightness temperature; 2) the impact of snow on-ice; 3) the impact of ice structure; 4) inter-comparison of radar and radiometer measurements of two missions – Jason and Sentinel-3; and 5) the spatio-temporal variability of Jason-2 waveforms. Finally, Section 4 summarizes the key findings and provides a brief description of the next steps to be completed in preparation of the Final Report.

1.3 Applicable documents

- Duguay, C.R., G. Picard, and E. Zakharova, 2020. Towards the retrieval of lake ice thickness from satellite altimetry missions (LIAM) - Scientific and Technical Report: State-of-the-art review, analysis and requirement review. ESA Contract No. 4000130930/20/I-DT.

- Proposal “Towards the retrieval of lake ice thickness from satellite altimetry missions”, Invitation to Tender AO/1-9101/17/I-NB, EO Science for Society Permanently Open call for proposals (EOEP-5 BLOCK 4).

2. FORWARD MODELLING OF BACKSCATTER AND BRIGHTNESS TEMPERATURE USING THE SMRT MODEL (WP 200)

2.1 Representation of lake ice and on-ice snow properties in SMRT

The representation of lake ice in the SMRT model is a key tool to perform meaningful sensitivity analysis. By representation we mean first the formulation or model that describes the electromagnetic signature (scattering, absorption, effective refractive index, ...) of each layer of the frozen lake environment (snow, snow ice, ice, water) and second, all values of the properties that describe in detail each layer of the medium (e.g. temperature, density, bubble size, roughness scale).

SMRT (Picard et al., 2018) offers a wide variety of different electromagnetic formulations to represent the medium; however the selection of the most suitable for each layer is a difficult task. The main choices are guided by: 1) the scattering theory; 2) which material is the scatterer, which one is the background host (between air, ice and water), knowing that SMRT only has two-phase scattering media; and 3) the rough surface model (Fresnel, Geometrical Optics, IEM, ...). As an example, to represent “normal” snow, we usually recommend the IBA scattering theory and either the Sticky Hard Sphere or Exponential microstructure (Picard et al., 2018). Representation of the microstructure then determines the type of “grain size and shape” metrics to provide to SMRT. Values for these metrics are required as input for each layer. Other properties, common to all microstructure and model, are the density and temperature. At this stage, for sensitivity analysis, we use “expert knowledge” to select these values.

Representing snow is becoming an issue that is increasingly being better mastered, thanks to the legacy of three decades of works, including the R & D activities that took place during the development of the CoReH2O satellite mission concept (ESA, 2012). CoReH2O, though not selected by ESA in the end, and more recent international research efforts have led to the development of SMRT. However, for the components of lake ice other than the overlying snow cover such as bubbly ice or snow ice, we have much less experience.

The following choices have been made to represent the different components of lake ice cover (Figures 2.1 to 2.3):

1. Bare clear (congelation) ice is represented as a stack of horizontal layers with a temperature profile. The addition of bubbles (represented as air spheres in an ice background) is possible. The parameters are the diameter of the bubbles and the ice density which determines the number density of air bubbles (Figure 2.1).

2. Water is represented as a boundary layer interface (Figure 2.1). The penetration of microwave into water is indeed shallow (due to high absorption) and the temperature is fairly constant over such a depth, so that it is not necessary to represent water with multiple layers. Modeling water as a boundary layer is equivalent to as a semi-infinite homogeneous layer of water, but is numerically more stable. The parameter is temperature.

3. In addition, the ice/water interface can be rough and/or contain bubbles (Figure 2.2). Roughness at this interface is in fact the most important contribution. It is indeed the main source of scattering (by far) and has a strong impact on backscatter.

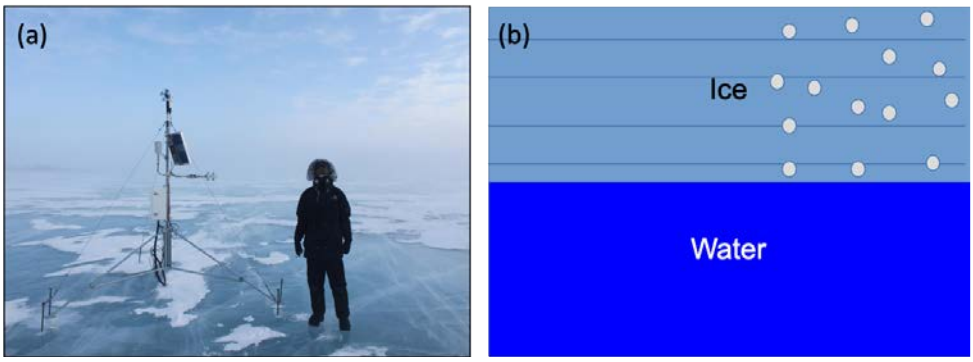

Figure 2.1. (a) Researcher and weather station standing on clear (congelation) ice with thin snow and snow-free areas, and (b) representation of clear ice as a stack of horizontal layers without and with the presence of air bubbles, and water as a boundary layer in SMRT. Note that the ice-water interface is a smooth interface in this example.

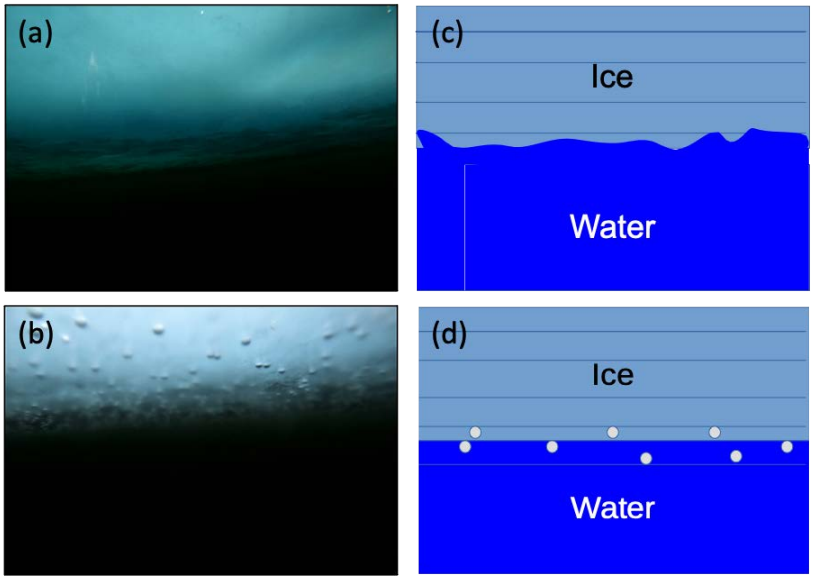

Figure 2.2. Photos taken with a digital camera deployed under the lake ice cover showing small roughness variations at the ice-water interface (a) without and (b) with the presence of air bubbles. (c) Representation of roughness at the ice-water interface and (d) bubbles at this interface (with a smooth interface in this example) in SMRT.

Given the typical roughness scale height (millimeters), the Integral Equation Model or IEM (Fung et al., 1992) is the most adequate among models available in SMRT. The parameters are the roughness height and horizontal correlation length. The implementation in SMRT only accounts for the backscatter return; bistatic scattering in the other directions is neglected. This means that multiple scattering between the ice-water interface and other scattering layers is absent from the simulations. To account for the presence of air bubbles in the ice, it is possible to add a layer of water with air inclusions (not tested yet). The parameters are water density (which determines the density of bubbles) and the bubble size.

4. Snow and snow ice (i.e. refrozen slush at the snow-ice interface) are modeled with different options according to the conditions (Figure 2.3). Dry snow is modeled by considering icy spheres embedded in an air background. Wet snow, when wetness is moderate is also modeled with spherical scatterers in air background, but the scatterers are made of mixed ice

and water (i.e. their permittivity is obtained by mixing pure ice and pure water permittivity in proportions according to the liquid water content using the Polden van Santen mixing formula (Sihvola, 1999). When melt is intense and water percolates down to an impermeable layer, or when the ice is flooded due to the load of the overlaying snow (negative freeboard), the porosity of snow can be filled, the air component becomes a minority and can be neglected. It is then more relevant to represent such snow as ice spheres in a water background.

When water refreezes, snow ice is formed (or superimposed ice when water comes from percolation instead of flooding at the ice-snow interface) (Figure 2.3). Snow ice has a complex structure with mainly ice and a bit of air (bubbles). The selected representation is air scatterers in an ice background, i.e. the same as to represent air bubble in the ice. This is not fully satisfactory because of the very different structure, but the characterization of snow ice microstructure had not been addressed up until now. Hence, the main uncertainty is probably elsewhere; knowledge of the basic parameters of the snow ice layer (its density, its thickness) is highly uncertain. However, the coupling of SMRT with the Canadian Lake Ice Model (CLIMo; Duguay et al., 2003) will help to alleviate some of this uncertainty since this model can simulate the evolution and thickness of snow ice layers.

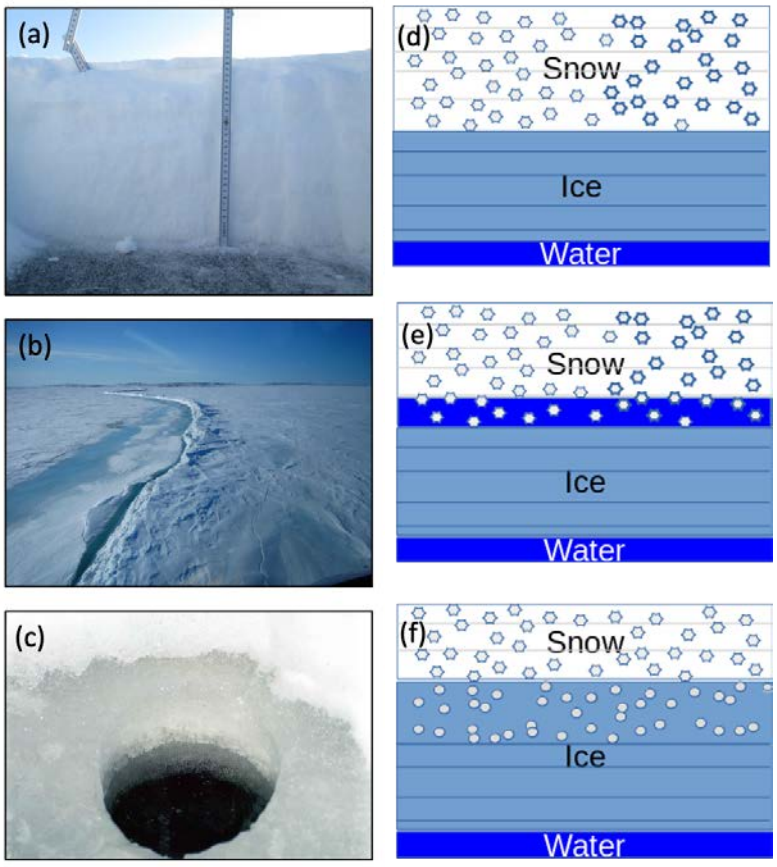

Figure 2.3. Photos on the left side show conditions that can be encountered on lake ice during winter: (a) snow on ice, (b) presence of a pressure ridge and flooded area to the left, and (c) presence of a snow ice layer between the overlying snowpack (slush at the base) and clear ice (darker ice layer in drilled hole). Figures on the right illustrate the representation of these properties in SMRT: (d) snow - clear ice - water layers, (e) snow - slush – clear ice - water layers, and (f) snow – (bubbly) snow ice - clear ice – water layers. Note that 3-D features such as the pressure ridge shown in (b), which is about 2 m in height (photo taken from helicopter), are not represented in SMRT.

Limitations:

There are a few major lake ice features that cannot be represented in SMRT.

Being fundamentally a 1-D model, SMRT cannot account for 3-D features such as pressure ridges and cracks in the ice. Backscatter (for side looking radar) is known to be sensitive to ridge slopes that offer a perpendicular surface to the radar, leading to high energy return. Cracks in the ice cannot be represented but are likely to contribute to scattering, as they are seen by the wave as a double rough interface potentially filled with water (high dielectric constant).

By 1-D model, it is usually meant that the snowpack has homogenous properties in the x,y directions. The roughness parameters (rms height and correlation length) are statistical properties that are homogeneous in the horizontal direction. It is not possible to explicitly describe the shape of the surface in a 1-D model like SMRT, which would require indeed a 2D or 3D model. In other words, the roughness itself is not represented in SMRT, only a statistical representation of it.

We also do not consider leads or surface heterogeneity. This would be possible in principle, as long as the horizontal scale of the leads or heterogeneity is much larger than the vertical scale (ice thickness). In this case, SMRT could be run for each surface type, independently, and the results averaged with weights corresponding to the relative areas covered by each type. This approach is known as “mixed pixels” and assumes a negligible horizontal interaction between the different surface types. However, here, for the sake of simplicity, and because the characterization of the environment is not precise, we only consider “pure” pixels (or footprints).

2.2 Forward simulations with SMRT in standalone mode

We first investigate the sensitivity of brightness temperature and backscatter to the main properties of the environment and, in particular, how the relation between the signal and ice thickness is affected by the presence of snow, snow ice, roughness, etc. We start from a fairly realistic but simplified medium description and we vary a single property over a possible range of values. We then analyze how much the satellite signal is affected by this property.

The typical environment is composed of two or three layers of clear ice with a temperature gradient as shown in Figure 2.4a. Permittivity is set to 1.60, 3.15 and 2.96 for snow, clear ice and snow ice layers, respectively. The permittivity values are not set but calculated by the model. Permittivity depends on temperature and density of each layer and on frequency. The other parameters, i.e. density and bubble size are kept constant. The bottom interface with water is rough, with a 1 mm RMS height in this example. On top of ice, we optionally introduce snow as a single layer (Figure 2.4a). We also optionally add snow ice as a single layer between the clear ice and the snow (Figure 2.4b).

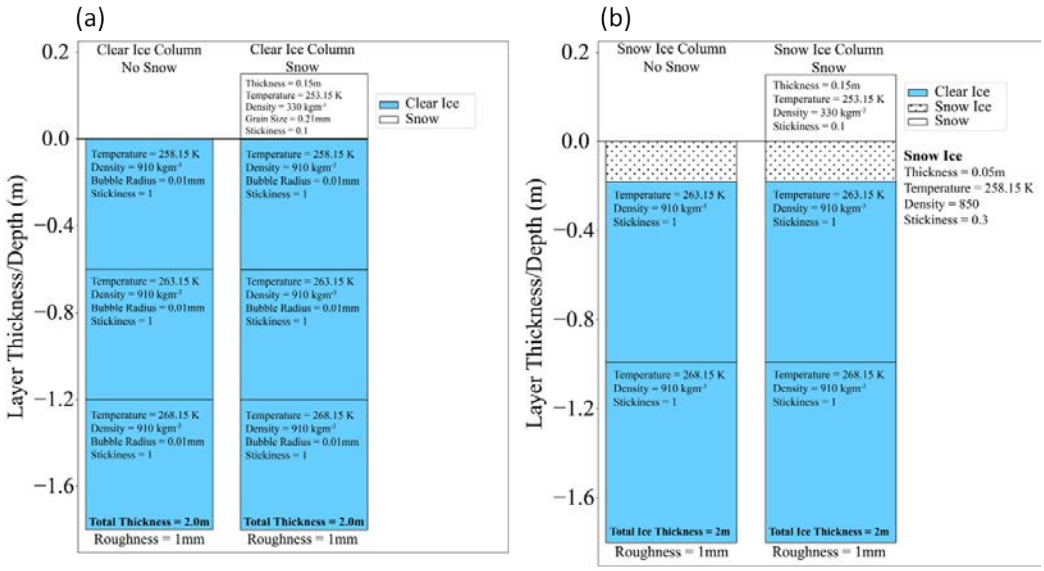

Figure 2.4. Example of scenarios used to investigate the sensitivity of brightness temperature and backscatter at frequencies of altimetry missions to lake ice properties.

The scenarios shown in Figure 2.4 are two cases representative of typical conditions that can be encountered on large northern lakes such as Great Slave Lake, Canada. For example, the snow stickiness of 0.1 is taken from Vargel et al. (2020) which is a typical value observed in the Arctic/sub-Arctic. It should be noted that the values of some parameters were modified from the cases shown in Figure 2.4, particularly when investigating the impact of that particular parameter on brightness temperature and backscatter. For example, in Figure 2.4, roughness at the ice-water interface is set to 1 mm. However, when examining the impact of roughness on the microwave signals, its value was changed accordingly. In the simulation results presented below, we shall illustrate when a change was made to any parameter from either of the baseline scenarios presented in Figure 2.4.

2.2.1 Sensitivity of brightness temperature to ice and on-ice snow properties

a) Ice thickness and snow depth:

The brightness temperature (Tb) increases with ice thickness, and the sensitivity highly depends on frequency (Figure 2.5). At 18.7 and 23.8 GHz the increase is relatively linear from 0 to 2 m ice thickness. At the higher frequencies (34.0 and 36.5 GHz), where penetration depth in clear ice is lower (see Figure A1 in Appendix), the signal saturates around 0.75 – 1 m. For thicker ice, the signal is constant or even slightly decreases due to the increasing contribution of the upper ice layer which is colder than the lower layers.

The presence of snow on the ice surface (constant 0.15 m snow depth for this scenario) results in a large increase of the Tb. This is likely due to the impedance matching. Snow has indeed a smaller permittivity than ice, which facilitates the transfer of radiation through the surface interface. These results for nadir (altimetry mission) observations would be different at 55° (e.g. AMSR-E/2; Kang et al., 2014) close to the Brewster angle and at V polarization where impedance matching has no impact. Even at the higher frequencies, the effect of snow scattering which would decrease the Tb is not visible. We can conclude that the main role of snow is due to impedance matching and the most critical parameter is therefore the density,

through its control on snow permittivity. This explains the weak sensitivity to snow depth (Figure 2.6).

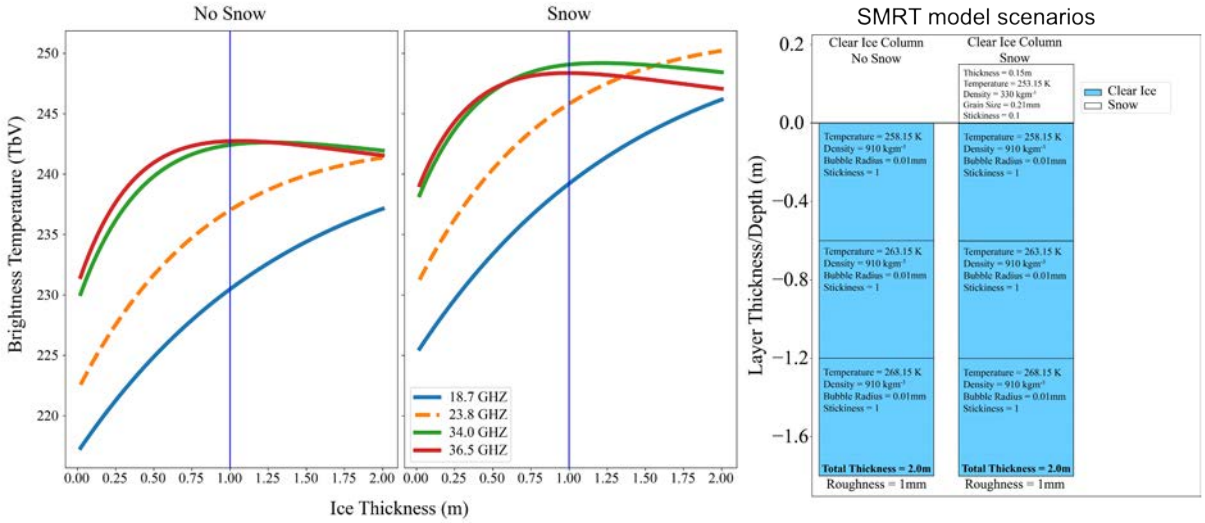

Figure 2.5. Sensitivity of Tb at different frequencies to ice thickness without snow and with snow on clear ice. The corresponding SMRT model scenarios are shown on the right.

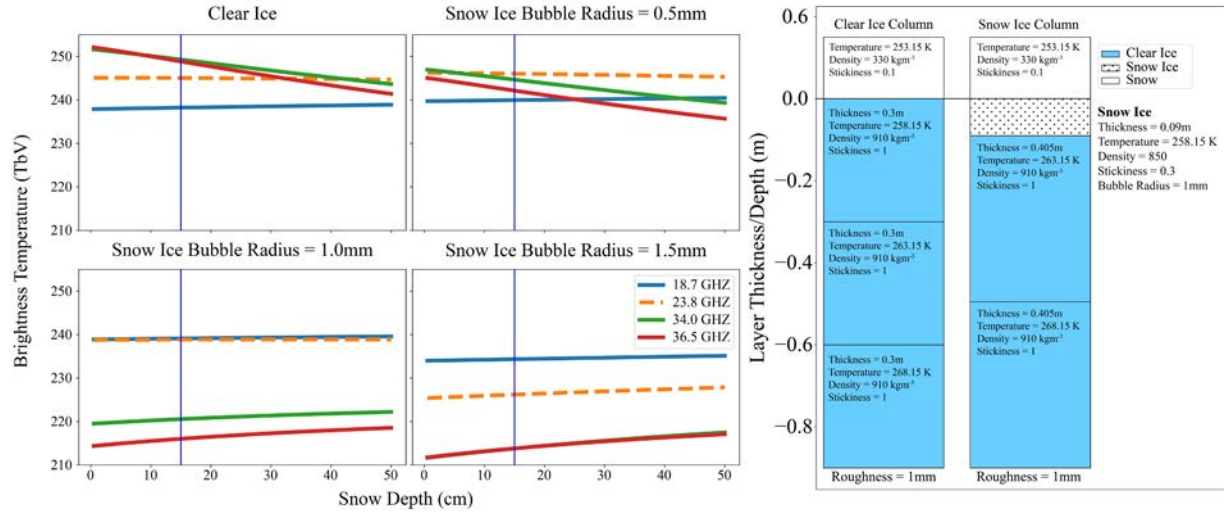

Figure 2.6. Sensitivity of Tb to snow depth overlying clear ice only and with the addition of a snow ice layer with varied bubble radii. The corresponding SMRT model scenarios are shown on the right.

These first results suggest that the Tb = f(ice thickness) relation at low frequency is somewhat disturbed by snow. However, by using the higher frequencies, it seems possible to “infer” the presence of snow, and use this information to determine the Tb = f(ice thickness) relation at low frequency. The combination of both lower and higher frequencies is therefore an avenue that should be explored for the retrieval of ice thickness.

b) The role of snow ice:

Snow ice can be a strong scattering medium due to the presence of large and numerous air bubbles. Results presented in Figure 2.7 indeed show that the Tb decreases with bubble size and the effect is much more significant at the higher frequencies. Both are a clear indication of this scattering effect.

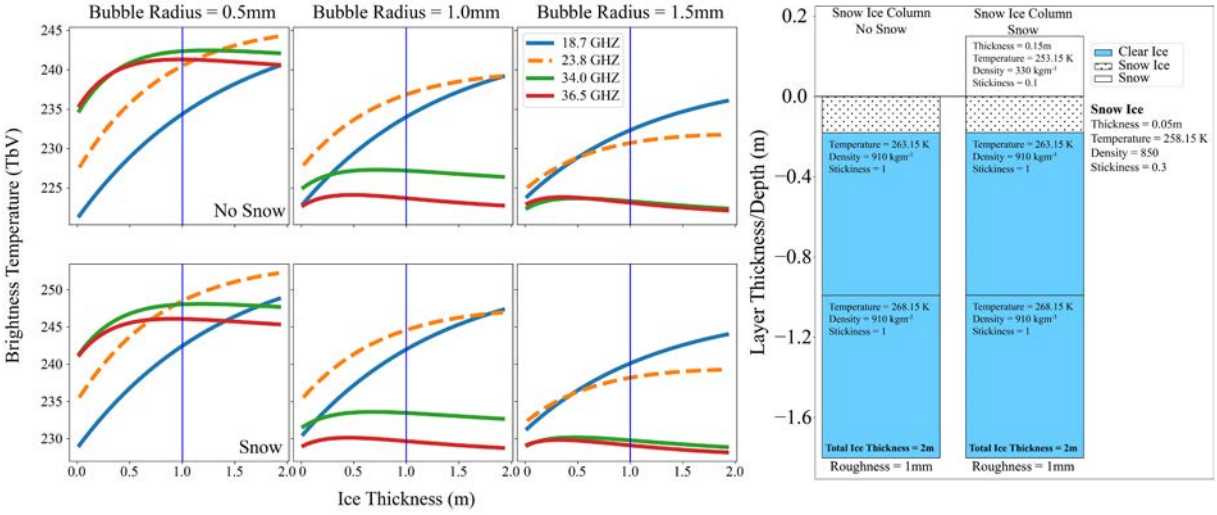

Figure 2.7. Influence of snow ice with three different bubble radii on the relation between Tb and ice thickness. The thickness of the snow ice layer is set at 0.05 m and with two evolving equal layers of clear ice. Simulations performed without (top) with snow (bottom) on the ice surface. The corresponding SMRT model scenarios are shown on the right.

While this affects the Tb = f(ice thickness) relation, here again we can see that the perturbing effect is more marked at the higher frequencies, which could then be exploited to correct from this effect at the low frequencies, in principle.

The possibility of correction is, however, limited. For a thick snow ice layer (here 10% of the total ice thickness), the effect becomes increasingly strong (Figure 2.8) such that the sensitivity to ice thickness is lost even at the lower frequencies. In all simulations investigating the role of snow ice on Tb and backscatter (see Section 2.2.2), 10% is set as an arbitrary value but it is nonetheless a realistic situation observed on high-latitude lakes (Brown and Duguay, 2011).

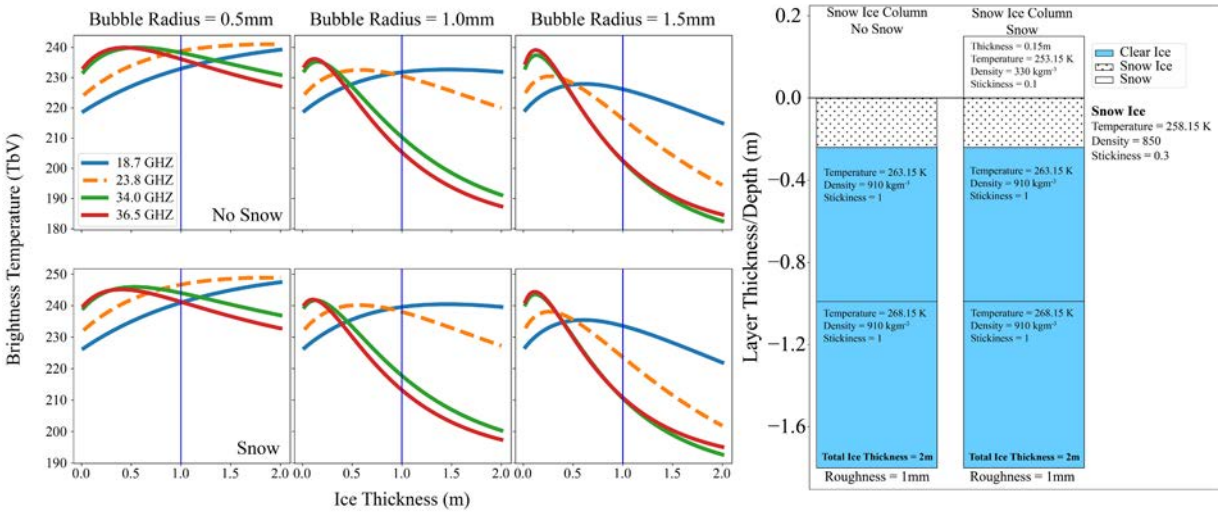

Figure 2.8. Influence of snow ice with three different bubble radii on the relation between Tb and ice thickness. The thickness of the snow ice layer is set to 10% of the total ice thickness with two equal evolving layers of clear ice. Simulations performed without (top) with snow (bottom) on the ice surface. The corresponding SMRT model scenarios are shown on the right.

c) Roughness at the ice-water interface:

The roughness at the ice-water interface plays a crucial role. In the absence of other strong scatterers (such as snow ice), the snow and ice behave mainly as a weakly absorbing media with reflection at the interface (result is more or less impedance matching). The main source of scattering is therefore the bottommost interface. This role is significant because between the ice (low permittivity, 3.15) and the water (very high permittivity, 88), the dielectric contrast is strong. Over the roughness range investigated in Figure 2.9, the effect of roughness is large and is more visible at the lower frequencies because the signal is coming from deeper than at higher frequencies. In practice, the expected natural variations of roughness is smaller than the range investigated in Figure 2.9, and a realistic value of roughness for passive microwave simulations is ~1 mm (Kang et al., 2014). Nevertheless, this value is critical to determine the Tb = f(ice thickness) relation. It must be known, and the higher frequencies are not useful for this.

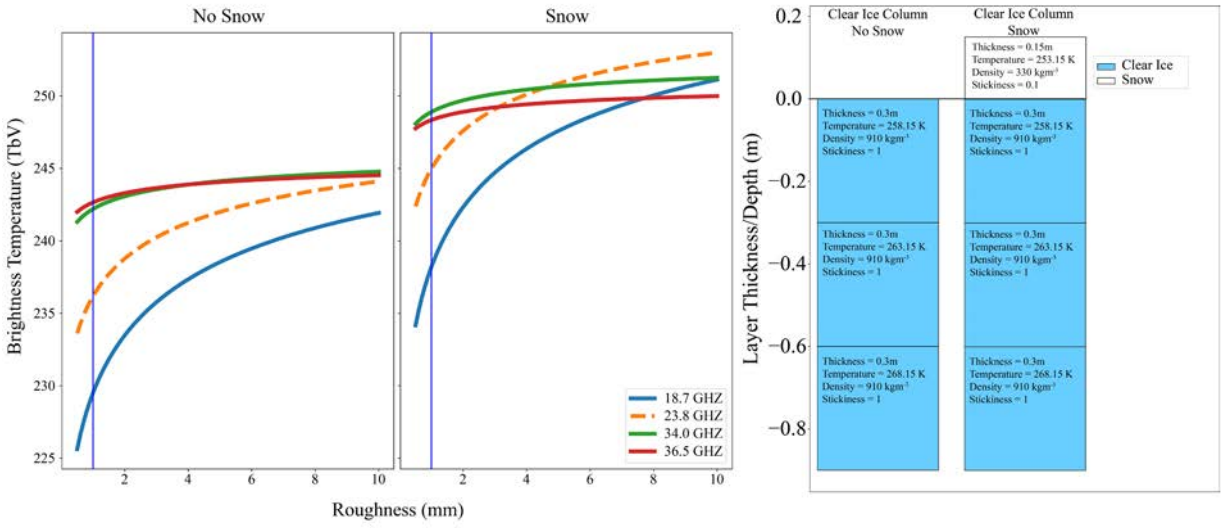

Figure 2.9. Sensitivity of Tb to roughness at the ice-water interface without snow and with snow on clear ice. The corresponding SMRT model scenarios are shown on the right.

d) Snow wetness:

The presence of liquid water in snow is known to greatly affect the microwave signals. The first effect, when snow gets wet is an increase of the absorption, which can make snow a nearly perfect blackbody. This leads to a sharp increase of the brightness temperature as shown in Figure 2.10. The quantity of liquid water required to observe a change is extremely small and the signal saturates for very tiny liquid water content. This means that: 1) the amount of liquid water cannot be retrieved; and 2) as soon as snow gets wet (T = 0°C) it is likely that the brightness temperature signal is affected and saturated. As a consequence of this highly absorbing snow layer, the signal coming from below is unable to escape the ice. The sensitivity to ice thickness and any other property of the ice vanishes.

For larger liquid water content, the simulation uses “ice in water” scatterers as explained above. The results (Figure 2.10) show that the signal decreases with increasing wetness. The reason of this reverse effect is that the snow layer becomes highly reflective, due to the higher permittivity of water compare to ice (or even air). In other words, the impedance matching is less efficient compared to with dry snow. Nevertheless, even if the high absorption does not drive the observed signal, it is still very significant and it results in the absence of sensitivity to any property of the medium property below the wet snow layer.

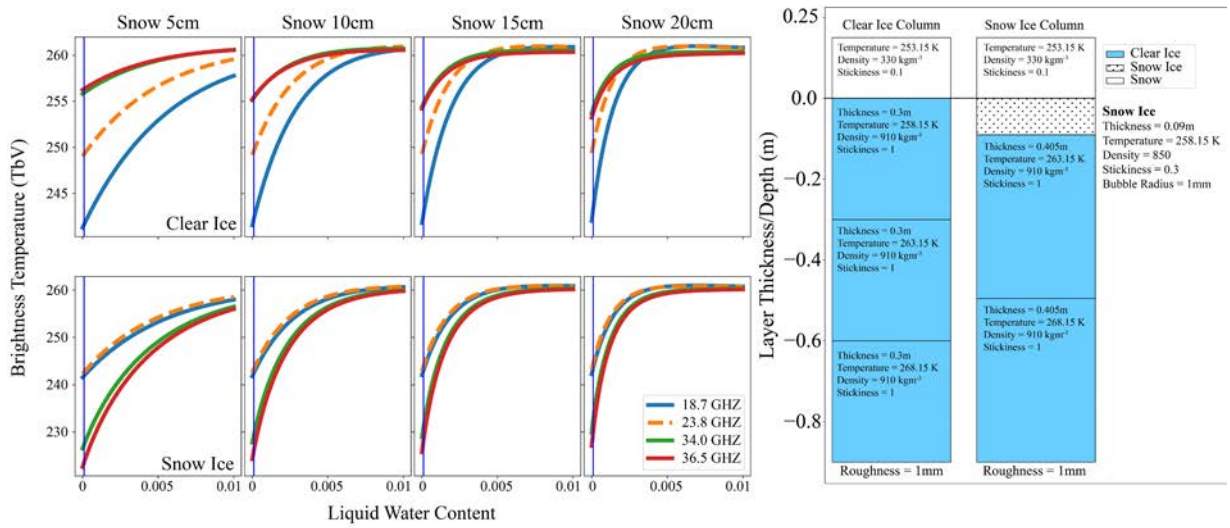

Figure 2.10. Sensitivity of Tb to liquid water content (0 to 1%) in snow of various depths over clear ice only and over layers consisting of snow ice and clear ice. The corresponding SMRT model scenarios are shown on the right.

2.2.2 Sensitivity of backscatter to ice and on-ice snow properties

The sensitivity of backscatter is investigated using the same approach as for brightness temperature described above. Because the same physical principles also apply, the wave-snow-ice interactions are largely independent on the source of the microwave emission (either the thermal emission or the radar pulse), so that the general features are relatively similar to those presented in the previous section. The main differences are due to the fact that: 1) backscatter is sensitive to some directional effects while brightness temperature integrates the emission from many angles; and 2) altimeters usually acquire data at lower frequencies than the passive microwave radiometers onboard altimeter missions.

a) Ice thickness:

Simulations show that backscatter over clear ice (with or without snow) is sensitive to the ice thickness only at Ku-band (Figure 2.11). At higher frequencies, the signal is attenuated before reaching the ice-water interface, which is the main source of scattering. The drop at Ka-band between no-snow and snow can be explained by some non-negligible scattering by snow. The incident signal is scattered during the downwelling and upwelling directions. The main echo comes from the snow layer.

At the lower frequencies, two effects combine: 1) the scattering of the ice-water interface is weak; and 2) the attenuation by the ice is too weak to induce a sensitivity to ice thickness. In other words, results suggest that Ku-band is an optimum frequency where scattering by the ice-water interface is strong enough to produce significant backscatter and the absorption is just the right magnitude to produce detectable variations (~ 2 dB) for an ice thickness range of 1-2 m.

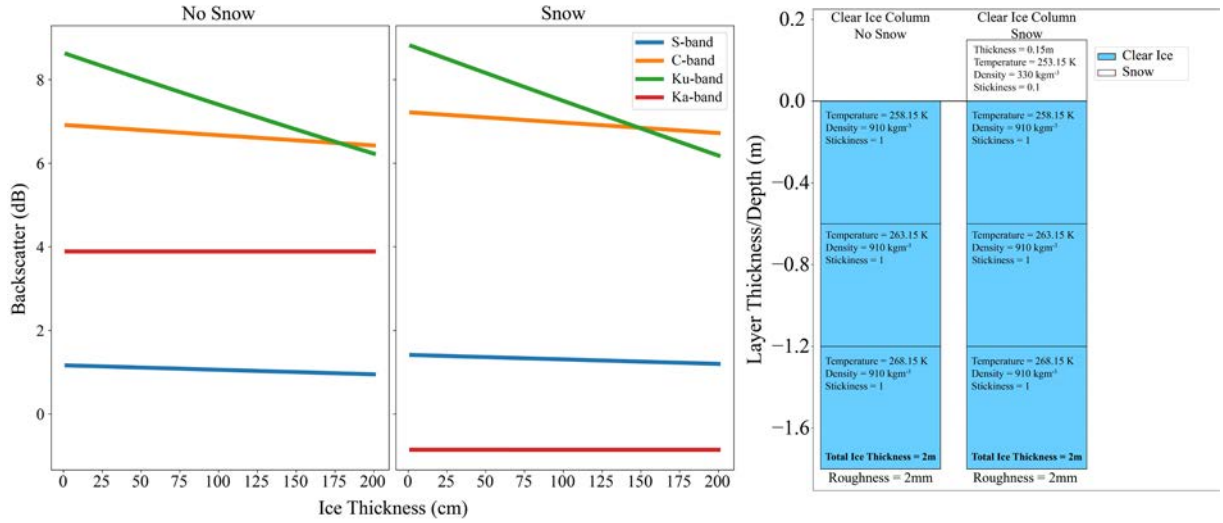

Figure 2.11. Sensitivity of backscatter at different frequencies to ice thickness without snow and with snow on clear ice. The corresponding SMRT model scenarios are shown on the right.

b) Ice type (clear ice and snow ice):

The presence of snow ice is also critical as it was for the passive microwave. Figure 2.12 shows how bubble size impacts the sensitivity of backscatter to ice thickness. The results show that the backscatter = f(ice thickness) becomes more and more sensitive as the bubble size increases at Ku band. To interpret these results, it is important to recall that the snow ice layer is 10% of the ice thickness, it is not constant over the ice thickness range. Snow ice is contributing to the Ku-band signal by attenuating the backscatter coming from the bottom ice-water interface, but it does not contribute through its own scattering. At Ka band, the signal increases with larger bubbles (i.e. more scattering), but there is virtually no sensitivity to the ice thickness because of the high absorption at this high frequency; no backscatter is coming from the bottom interface.

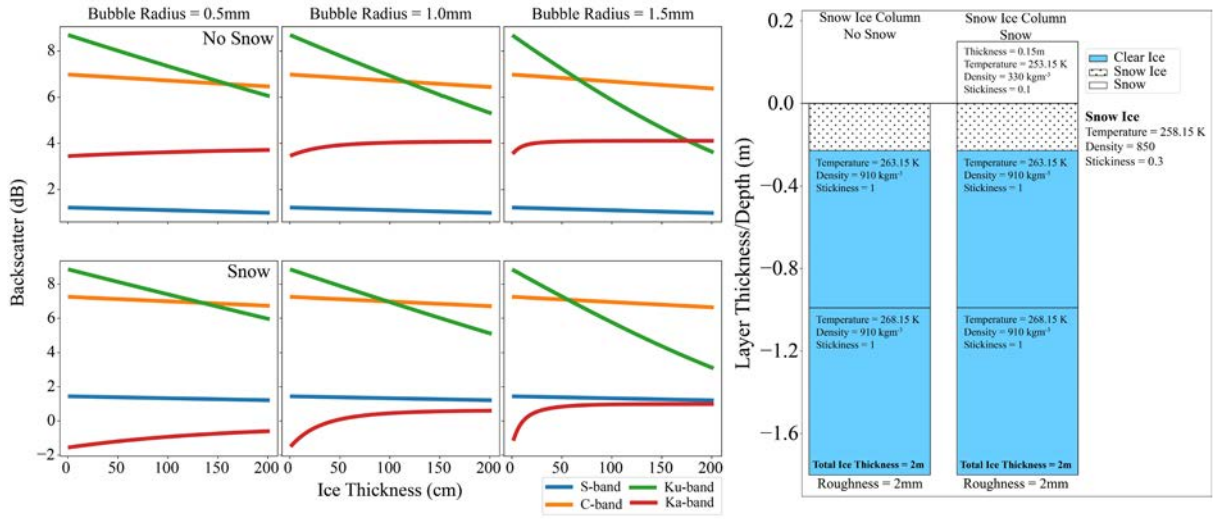

Figure 2.12. Influence of snow ice with three different bubble radii on the relation between backscatter and ice thickness. The thickness of the snow ice layer is set to 10% of the total ice thickness with two equal evolving layers of clear ice. Simulations performed without (top) with snow (bottom) on the ice surface. The corresponding SMRT model scenarios are shown on the right.

c) Roughness at the ice-water interface:

The ice-water interface is the main source of scattering and the dependency to roughness is significant at Ku-band and lower frequencies. This is the most crucial issue to address to exploit Ku-band backscatter for the retrieval of ice thickness. Some knowledge of the bottom roughness is required. Here we can see that C and S-band are even more sensitive to the roughness of the bottom interface (Figure 2.13), and may then serve to retrieve this information, as these bands have little dependency on ice thickness.

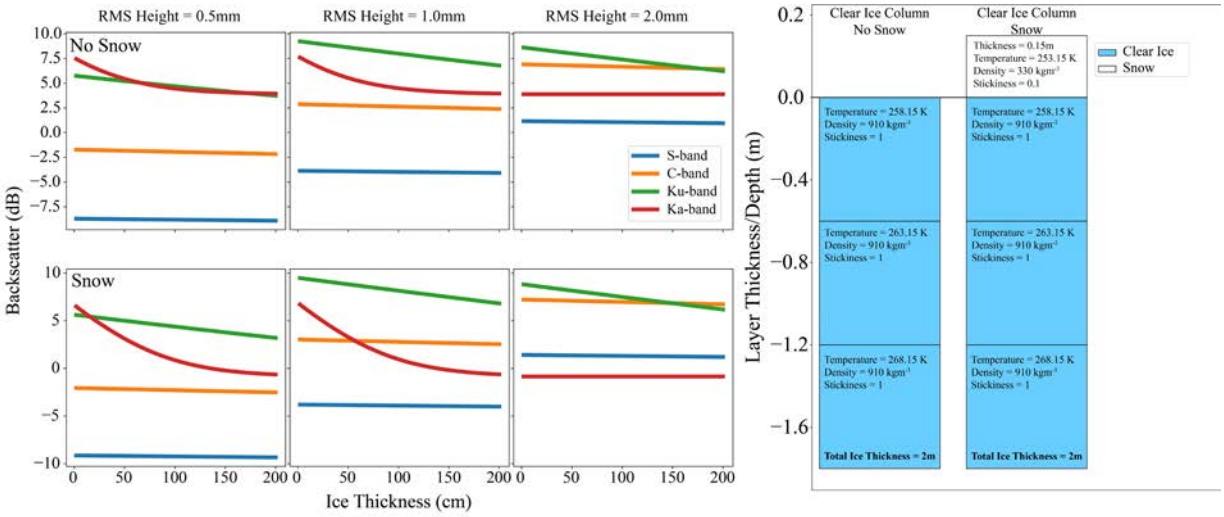

Figure 2.13. Influence of roughness at the ice-water interface (three RMS heights) on the relation between backscatter and ice thickness. Simulations performed without (top) with snow (bottom) on clear ice. The corresponding SMRT model scenarios are shown on the right.

2.3 Altimetric waveform simulations

A first series of simulations has been performed with the newly implemented altimeter module in SMRT. Results at S and Ku-band are shown in Figure 2.14. At the lower frequency, the echo is mainly coming from the bottom ice-water interface so that the leading edge gives the position of the bottom of the ice. At Ku-band the signal is more complex. With the first simulations, we show a two-step leading edge for the thicker ice (150 cm), which is caused by a first interface (likely the snow/ice interface) and the bottom interface. For thinner ice, the two echoes are too close to be separated, but in principle both interfaces contribute to the leading edge so that some uncertainty can come from this more complex situation. Further simulations are needed with thicker ice and by varying the snow and ice properties to assess how the steps change. Results from such simulations will be provided in the final report.

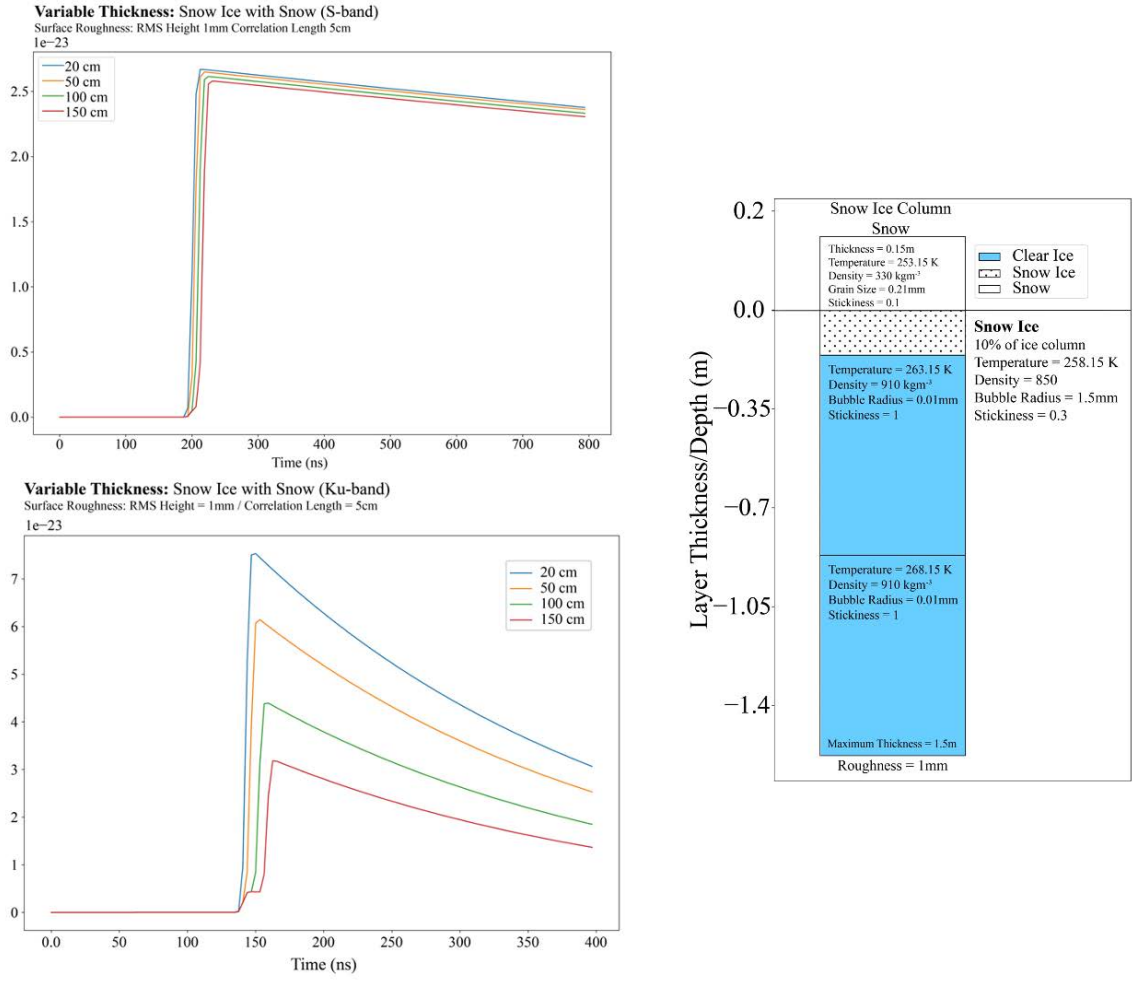

Figure 2.14. SMRT simulations of waveforms at S and Ku-band for varying total ice thicknesses. Snow depth is fixed at 0.15 m and the thickness of the snow ice layer is set to 10% of the total ice thickness. The corresponding SMRT model scenarios are shown on the right.

2.4 Coupling of CLIMo with SMRT

The aim of coupling CLIMo with SMRT is to provide a first guess of the backscatter or the brightness temperature from near-surface meteorological series. CLIMo can provide as output many of the properties required by SMRT as inputs (Figure 2.15). Some challenges in the coupling of CLIMo with SMRT are to:

1) Select (dynamically) the most appropriate representation of each layer of the frozen lake medium. Depending on the cases, different representations can be selected from SMRT and some are more appropriate than others. This task builds on the approach taken for the sensitivity analysis. The most delicate part concerns snow ice and wet snow.

2) Ensure that outputs from CLIMo and inputs of SMRT are well connected. The layering of CLIMo is applied to SMRT; only very small layers should be avoided in SMRT for its numerical stability. What is meant is that the lower thickness limit for a layer is the wavelength. The other main variable is the temperature, which is not subject to any ambiguity and can be directly connected between the models.

3) Estimate a few variables a priori. This is the case for snow density, grain size, bubble size. The values are based on the values use for the sensitivity analysis but of course this part is subject to large uncertainties.

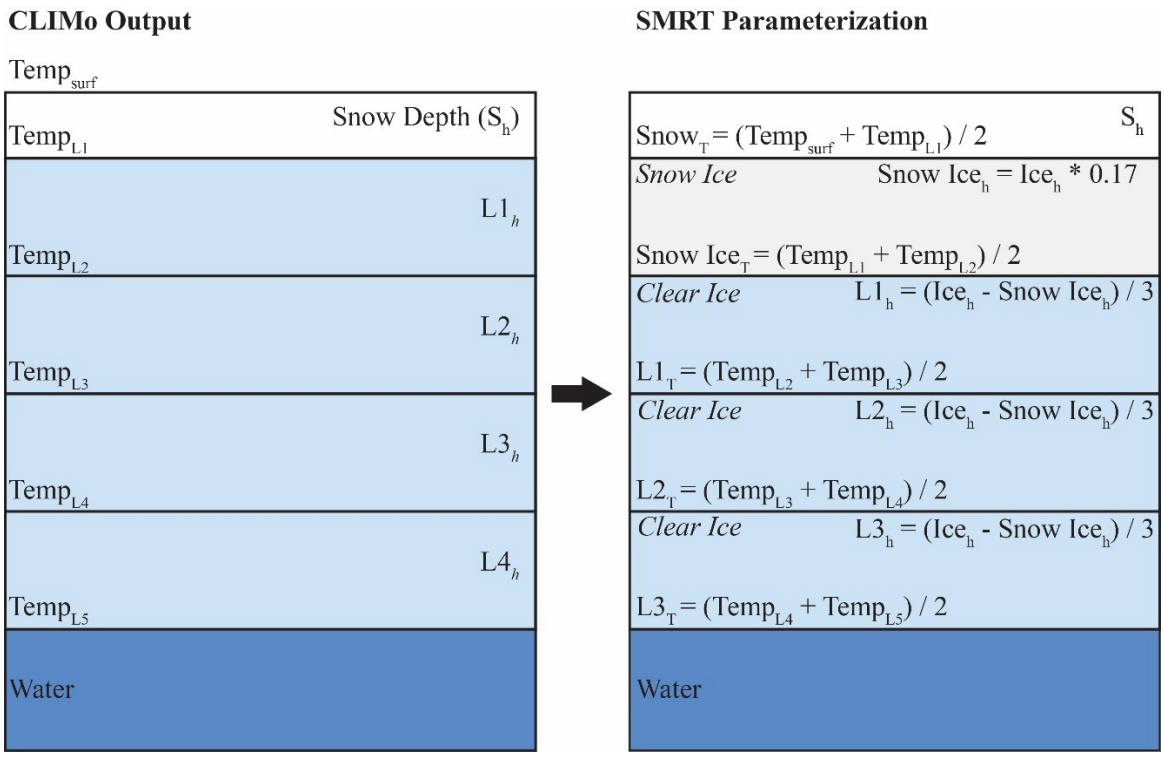

Figure 2.15. Coupling of CLIMo with SMRT. Ice_h corresponds to the total ice thickness.

The coupling of CLIMo with SMRT has now been achieved. One of the next steps of this study will be to perform coupled simulations. Results will be presented in the project's final report.

3. ANALYSIS OF ALTIMETRY AND RADIOMETER DATA OVER LAKES (WP 310)

Examination of the behavior of altimetric and radiometric signals over lake ice was performed using measurements from Jason-2/3 and Sentinel 3-A. Jason-2 (no longer operating since October 2019) and Jason-3 are equipped with dual-frequency (Ku-band/13.6 and C-band/5.3 GHz) conventional radar altimeter and three-band radiometer (18.7, 23.8, 34.0 GHz) radiometer. Sentinel-3 carries a dual-frequency (Ku and C bands) SAR altimeter and dual-frequency (23.8 and 36.5 GHz) passive microwave radiometer.

For inland water studies, the concept of the main contributing area is important as the size of waterbodies is often less than that of the satellite instrument's footprint. The footprints of radar and radiometer instruments depend on the frequency used and on instrument design (conventional or SAR). For the Jason series, the diameter of the radar footprint at Ku-band is between 2 and 12 km (depending on the surface roughness), while it is 42, 35, and 22 km in diameter for its radiometers operating at 18.7, 23.8, 34.0 GHz, respectively. The radar footprint over smooth ice surfaces is smaller and the main return echo can come from an area of 2-5 km in diameter.

We have investigated several questions specifically in relation to lake targets and their ice cover: 1) the impact of land contamination on measurements of radar backscatter and brightness temperature, 2) the impact of snow on-ice; 3) the impact of ice structure; 4) inter-comparison of radar and radiometer measurements of two missions – Jason and Sentinel-3; and 5) the spatio-temporal variability of Jason-2 waveforms (WF) has a precursor to future comparisons with WF reproduced by the SMRT model (WP 320) to be described in the final report.

3.1 Impact of land on backscatter and brightness temperature

Islands and their grouping complicate the interpretation of satellite measurements coming from such complex environmental patterns. Several factors can impact satellite measurements in the near-shore area: 1) bank type (flat/rocky, dry-flat/wet-flat) and 2) ice cover properties. The bank type defines a contrast between measurements acquired over lake ice and over land, while near-land ice cover properties can attenuate this contrast and result in masking the land effect. High relief (~800 - 1000 m) can lead to the loss of radar measurements over coastal ice up to 2.5 km (on Lake Baikal, for example). Over flat banks occupied by wet areas (bogs or small lakes) in the middle of winter, the satellite radiometer measurements can be close to those acquired over the lake ice. Two cases depicting the impact of variable land effects on radar backscatter measurements due to specific ice properties were observed in coastal areas. Firstly, depending on weather conditions at the beginning of lake ice formation, a flat (smooth) ice with specular properties (similar to sea ice formed in the leads) can form in near-shore areas after wind induced ice drift. This type of ice is characterized by higher backscatter values compared to the values observed over the main ice field. Secondly, higher near-shore snow accumulation due to wind can result in lower backscatter over coastal ice and extend the length of transition from land-typical to ice-typical backscatter values.

Our estimations show that, depending on the situations described above, the land effect characterized by a gradual decrease in backscatter can be observed from 1.5 to 4 km from the coast at Ku-band from both Jason-2 and Sentinel-3. In most cases, the C-band backscatter follows the same behavior as Ku-band backscatter. A few exceptions were noted for Lake Baikal's coastal area, where the land effect at C-band for particular sites and cycles seems to

appear 1-1.5 km away from the coast compared to Ku-band. However, we attribute this effect to the properties of the near-shore ice which introduce some differences in Ku and C-band measurements (Figure 3.1).

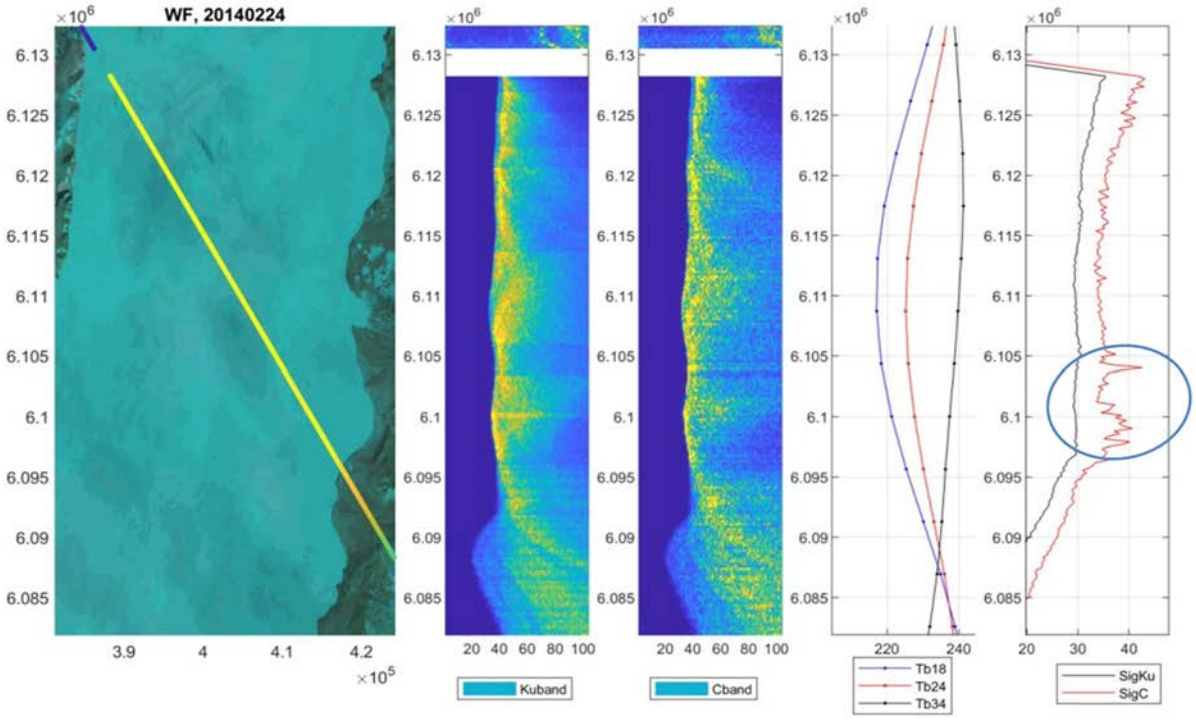

Figure 3.1. Jason-2 measurements over Lake Baikal showing a different behavior in Sig0 at Ku and C-band in the coastal area (blue circle). Coordinates are given in meters (UTM coordinates).

For cases where there is a high contrast between land and ice (> 20°K), the land effect can be negligible on brightness temperature (Tb) measurements of Sentinel-3 at 37 GHz (< 2°K) at 10-17 km away from the coast and it fully disappears at 18-20 km distance. In cases when the satellite track is parallel to the coast (Figure 3.2; Great Bear Lake), a decrease of 2°K is observed at a distance of 12 km from the coast. In cases of low land/ice contrast (< 10°K), Tb measurements at 37 GHz are not affected by land at a 10-km distance and even at 2 km in particular case of specular snow-free ice cover on Lake Baikal.

At 24 GHz, the land effect on Tb measurements over lake ice (in the cases of high land/ice contrast) fully disappears at 18-20 km from banks. At a distance of 14-15 km, this effect is less than 2°K. When the land/ice contrast is low, the land does not produce any effect on the Tb measurements already at a distance of 12 km from the coast.

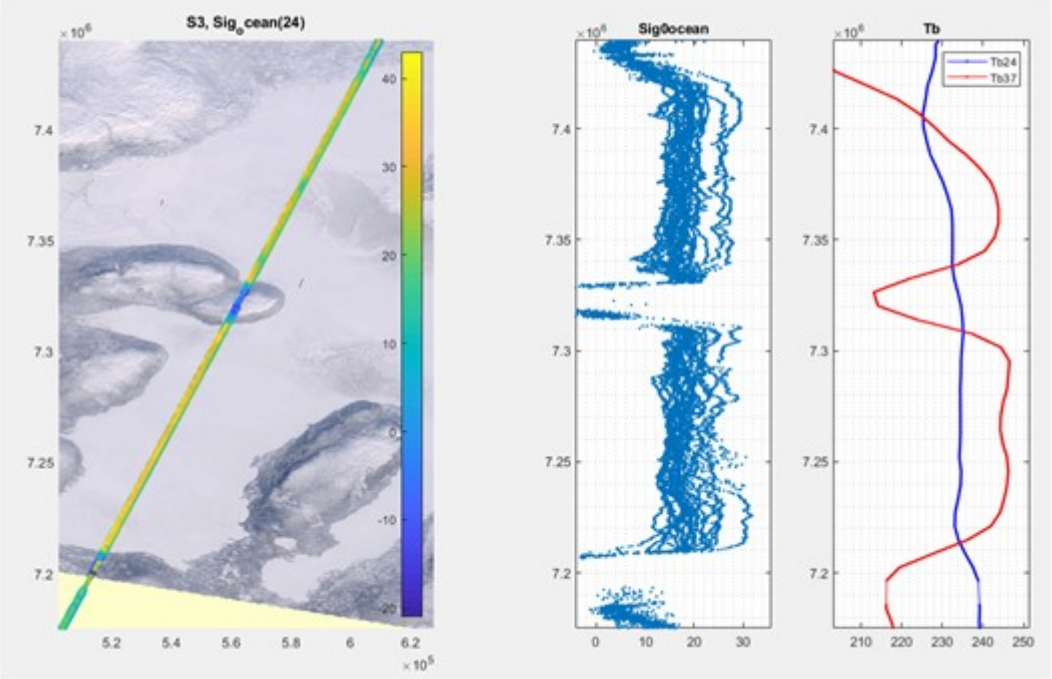

Figure 3.2. Sentinel-3A measurements over Great Bear Lake in February 2017 demonstrating the land effect on Ku-band Sig0 and for two land/ice Tb contrast cases. The distance on MODIS image and on y-axis is provided in UTM coordinates (meters). On the northern shore of the lake, the land effect on the Tb measurements at 37 GHz is likely masked by the decreasing emission of snow-free area between 7365000-7380000 m UTM latitudes and likely specific properties of ice in Dease Arm Bay (south part of Great Bear Lake).

3.2 Impact of snow on brightness temperature and backscatter

The effect of snow on backscatter and the brightness temperature measurements can be studied using two approaches: 1) by comparing the signal coming from snow-covered and snow-free lake ice; and 2) by comparing the Sig0 and Tb measurements made over the lakes (or lake parts) known to have thicker/thinner snow cover. In both approaches, the period starting with the initial lake ice formation should be considered since ice growth (thickness) may be masked by the effect of snow on the ice surface depending on frequency.

Through the first approach, using Jason-2 measurements over Lake Baikal (known for its irregular spatial distribution of snow), we find that snow depth of the order of 20-80 cm results in a 2-3 dB decrease in Sig0 measurements at both Ku and C-band (Figure 3.3).

(a)

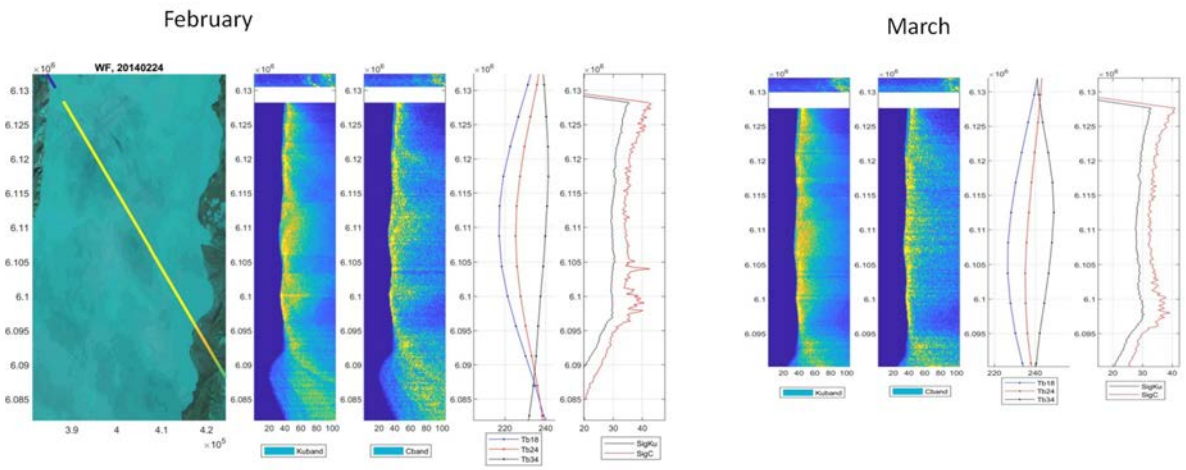

(b)

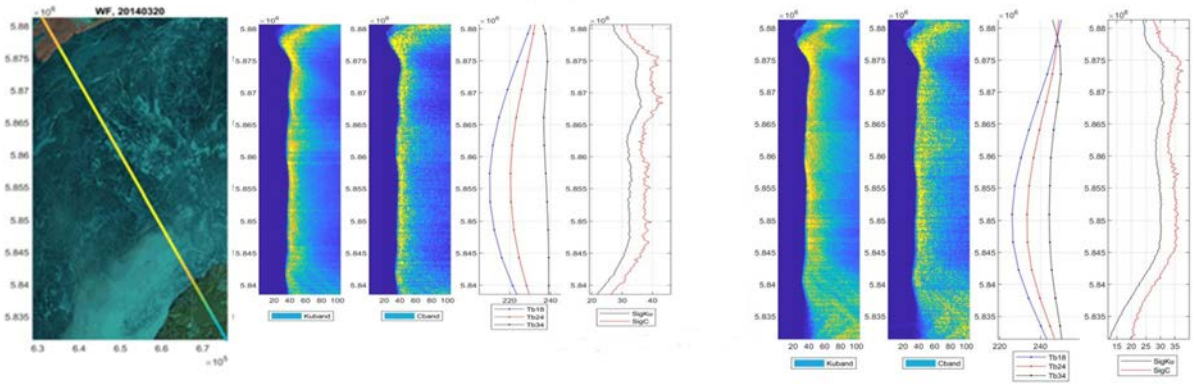

Figure 3.3. Jason-2 measurements over (a) snow-covered and (b) snow-free ice on Lake Baikal in February (left plots) and March (right plots) 2014.

The effect of snow on the radiometric measurements differs depending on the frequency used and likely on the ice thickness. When the ice is thinner earlier in the ice season, snow increases the emission by 6°K at 18 GHz and 24 GHz, and by 4°K at 34 GHz (Table 3.1). One month later, the difference in Tb between snow-covered and snow-free clear ice disappears at 18 GHz and reduces by 2-3°K at 24 and 37 GHz.

Table 3.1. Jason-2 measurements over Lake Baikal on 24 February 2014 (in numerator) and 20 March 2014 (in denominator) over snow-covered and snow-free lake ice areas located > 20 km away from the shore.

	Sig0 Ku (dB)	Sig0 C (dB)	Tb 18GHz (°K)	Tb 24 GHz (°K)	Tb 34 GHz (°K)
Snow-covered ice	30/27	35/33	216/226	226/235	242/248
Snow-free ice	33/30	38/35	210/226	220/233	238/245

The difference observed, nevertheless, cannot be fully attributed to the effect of snow. The impact of the difference in ice thickness between two areas cannot be excluded as the ice onset in the snowy area in 2014 occurred 20 days earlier. However, considering that the insulation effect of snow reduces ice growth, the difference in ice thickness between the snow-

covered and snow-free areas is expected to be low.

The second approach is based on analysis of monthly histograms of backscatter and brightness temperature constructed for Great Bear, Great Slave, Baker and Baikal using Sentinel-3A measurements (Figures 3.4 to 3.8). The ice on the Great Slave and Baker lakes, as well as of the northern part of Lake Baikal and the bays of the Great Bear Lake is covered by snow cover of variable depths. Following an analysis of MODIS images, we suggest that on-ice snow depth is low in the central part of Great Bear Lake (see areas with lower reflectance on MODIS color composite, Figure 3.2 above). However, according to historical archives (Kouraev et al., 2008), snow depth on ice can reach as much as 80-100 cm in the northern part of Lake Baikal, often as bands in near-coastal areas due to wind effects. This tends to be the exception rather than a generalization.

Sentinel-3A backscatter coefficients derived using the Ocean retracker exhibit less noise and better stability. Sig0 from the Offset Centre of Gravity (OCOG) retracker shows a systematic shift after 2020 and, thus, is not suitable for analysis (see upper right plots on Figures 3.4 to 3.8). The histograms are calculated using data from 2016-2020 with 20 Hz measurements for both Sig0 and Tb parameters from 2-4 tracks (Table 3.2). Apart from Baker Lake, which is smaller in area (ca. 40 km x 70 km with an island close to the centre), all selected measurements are located at least 20-25 km from lake shores. For Baker Lake, where the lake-Sentinel-3A cross-over length is 15-20 km, the criteria were reduced to 8-10 km. The brightness temperatures were spline interpolated from 1 Hz measurements.

Table 3.2. Sentinel-3A tracks used for histograms presented on Figures 3.4-3.8. Tracks for each lake are shown in Appendix (Figure A2).

Lake	**Track number**
Great Slave Lake	13, 18, 341, 346
Great Bear Lake	99, 156, 232, 289
Baker Lake	174, 269
Lake Baikal	209, 323, 95, 366

The multimodal shape of the histograms reflects both inter-annual and spatial variability of ice/snow conditions on lake ice and demonstrates that the mean monthly value is likely not a good statistic to assess the effect of snow cover. For simplification, considering only the second and third months from ice onset (January-February for Canadian lakes and February-March for Lake Baikal), we can provide some support to our earlier suggestion about the effect of snow on altimetric and radiometric satellite measurements over lake ice. Suggesting that on-ice snow depth decreases in sequence from Great Slave Lake/Baker Lake to Great Bear Lake/Northern Lake Baikal to Central Lake Baikal, which is likely associated with thicker ice cover, we observe a corresponding increase in the first modes of Sig0 in Ku band from the 2nd ice to the 3^{d} ice month (Table 3.3). The increase in ice emission, hence Tb, associated with the snow contribution is not straightforward when relying on the mode values for interpretation because of the multimodal Tb distribution. The increase in Tb is more distinct at the 24 GHz frequency, which is characterized by a greater penetration depth in snow/ice. However, the increase is questionable at the 37 GHz frequency. We will be able to provide a clearer explanation for this later in the project, after completion of WP 320 (Comparison of SMRT simulations with altimetry and radiometer data) and following the analysis of additional Sentinel-3 observations from Lake Baikal as well as from Jason-2/3 over all lakes.

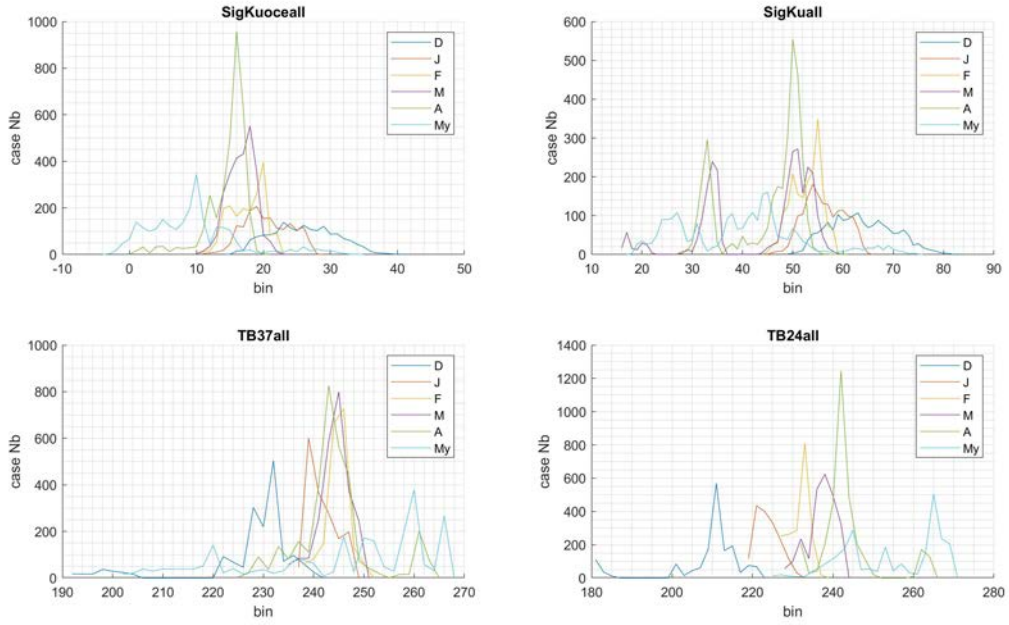

Figure 3.4. Monthly histograms of Sig0_Ku (top left: Ocean retracker, top right: OCOG retracker), Tb 37 GHz (bottom left) and Tb 24 GHz (bottom right) for Great Bear Lake (Canada). The colored curves correspond to months of the ice season (December to May).

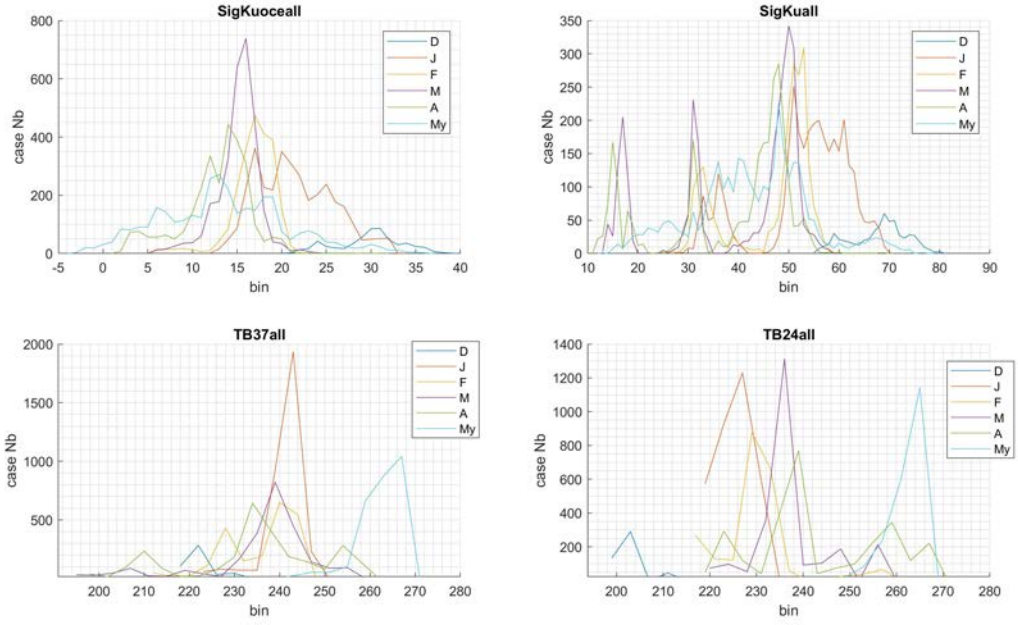

Figure 3.5. Monthly histograms of Sig0_Ku (top left: Ocean retracker, top right: OCOG retracker), Tb 37 GHz (bottom left) and Tb 24 GHz (bottom right) for Great Slave Lake (Canada). The colored curves correspond to months of the ice season (December to May).

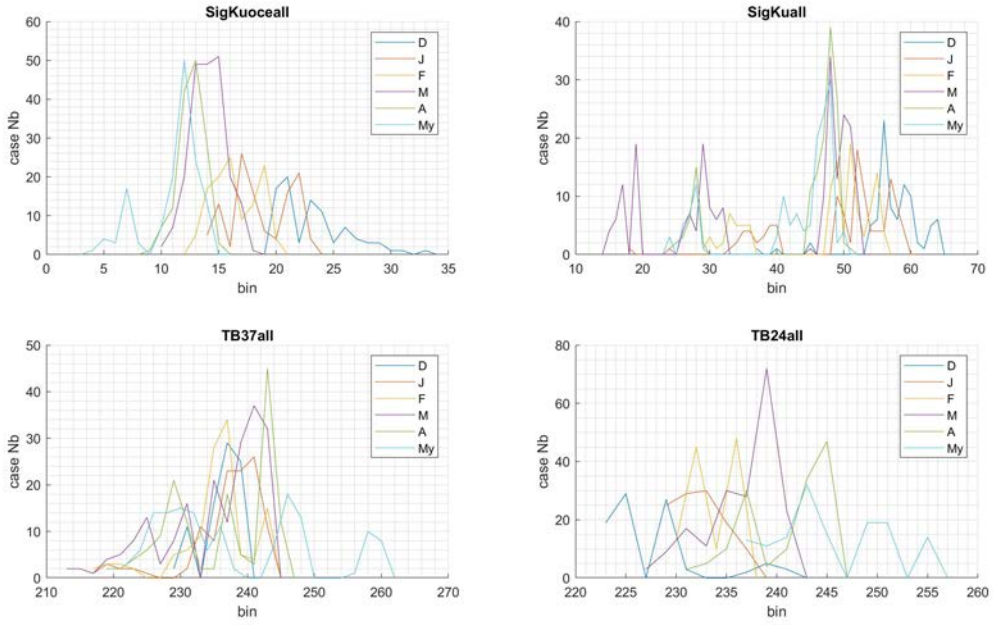

Figure 3.6. Monthly histograms of Sig0_Ku (top left: Ocean retracker, top right: OCOG retracker), Tb 37 GHz (bottom left) and Tb 24 GHz (bottom right) for Baker Lake (Canada). The colored curves correspond to months of the ice season (December to May).

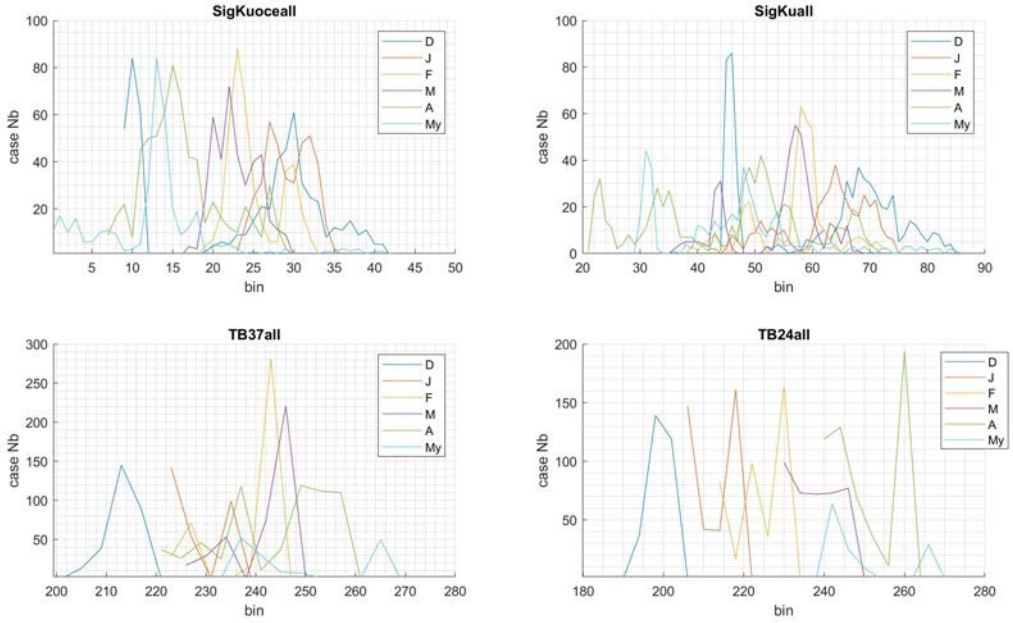

Figure 3.7. Monthly histograms of Sig0_Ku (top left: Ocean retracker, top right: OCOG retracker), Tb 37 GHz (bottom left) and Tb 24 GHz (bottom right) for Lake Baikal with thick snow cover. The colored curves correspond to months of the ice season (December to May).

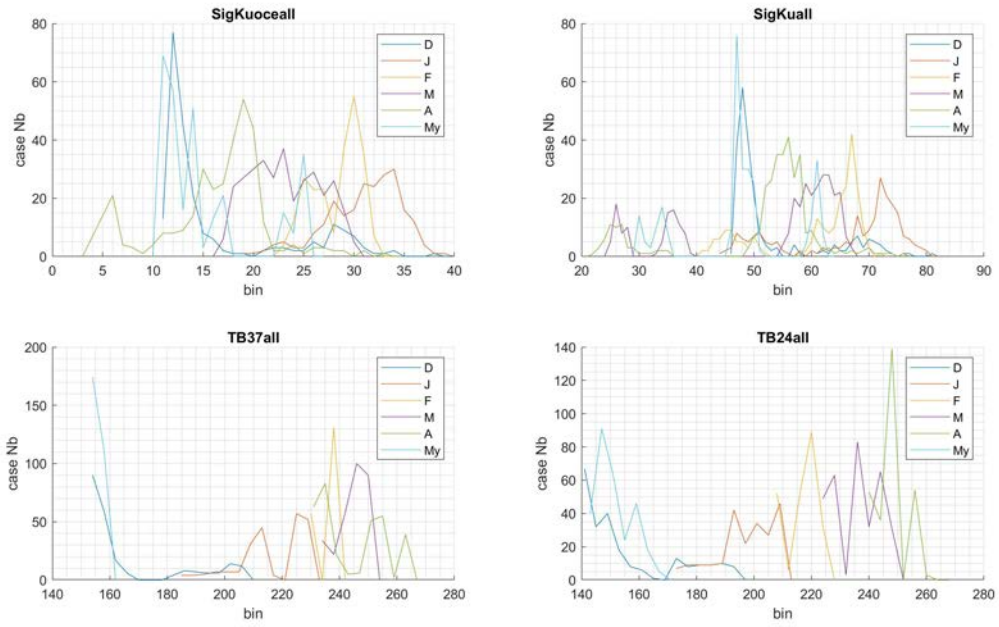

Figure 3.8. Monthly histograms of Sig0_Ku (top left: Ocean retracker, top right: OCOG retracker), Tb 37 GHz (bottom left) and Tb 24 GHz (bottom right) for Lake Baikal with snow-free ice. The colored curves correspond to months of the ice season (December to May).

Table 3.3. Sentinel-3A first monthly modes for lake ice with varied snow depth. Snow depth is assumed to decrease in the following sequence [**GSL/Bak** : **GB/NBa** : **CBa**]*.

Parameter	2nd ice month	3rd ice month
Sig0 Ku (dB)	[17dB : 19/23dB : 30dB]	[16dB : 20/22dB : 23dB]
Tb 24 GHz (°K)	[229/232°K : 233/230°K : 220°K]	[236/239°K : 237/230°K : 226/237°K]
Tb 37 GHz (°K)	[243/237 : 239/237°K: 237°K]	[240°K : 246°K : 246°K]

*Great Bear L. (**GB**), Great Slave L. (**GSL**), Baker L. (**Bak**), Northern Baikal (**NBa**), Central Baikal (**CBa**)

3.3 Impact of ice structure on brightness temperature and backscatter

In the absence of detailed ground truth measurements of the ice properties (bubble content, layering, bottom and surface roughness) over large areas of the lakes, the only parameters that we can potentially assess with combination of different remote sensing instruments (imaging SAR, optical, altimeters) are deformation features (i.e. cracks in the ice and pressure ridges). Simulations with the SMRT model do permit to examine the impact of properties such as bubble content, layering of ice and overlying snow, and roughness at the ice/water interface, but not deformation features which are 3-dimensional in nature (see Section 2.1 for details). Hence, the joint analysis of measurements from imaging sensors and SMRT provide an opportunity to assess the impact of simpler and complex ice properties that will be covered in the final report following completion of WP 320.

Lake ice, particularly at the beginning of ice formation, is usually smooth. However, during ice freeze-up floes can juxtapose on the ice edge. Moreover, during all winter months long pressure ridges can also form, thus increasing surface roughness. All irregularities on the

ice surface serve as a snow trap and, in fractured areas, snow depth is expected to be higher (based on field observations by team members). Using along-track histograms constructed for a 1-km moving window from winter measurements, we can define areas that could be considered as homogeneous in terms of ice spatio-temporal evolution (Figure 3.9) and use these for the selection of (quasi) homogeneous ice fields for statistical analysis, and eventually coupled CLIMo-SMRT simulations.

(a)

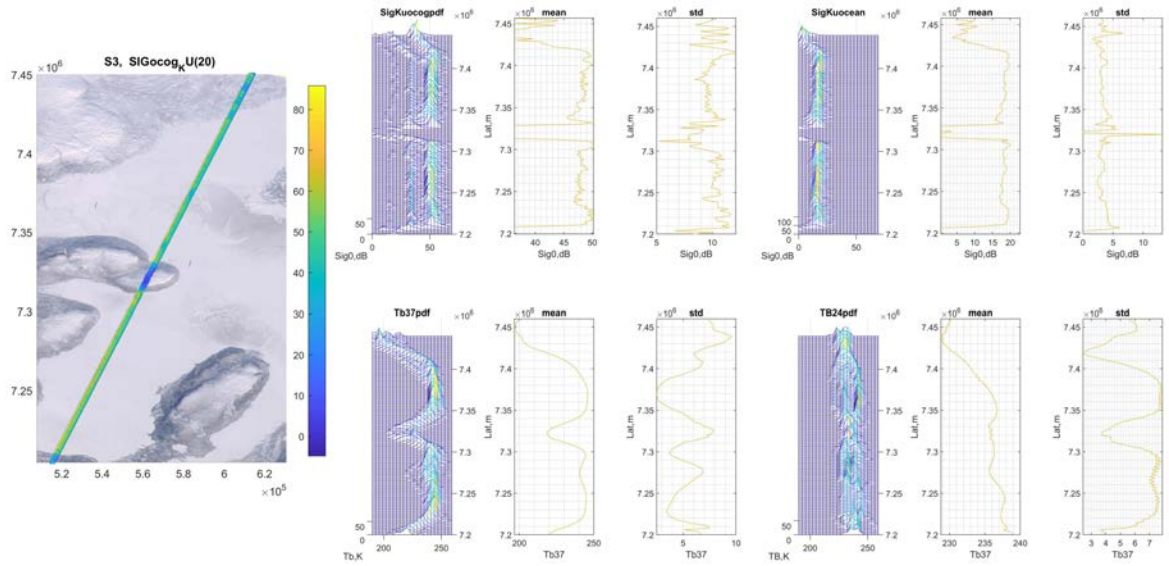

(b)

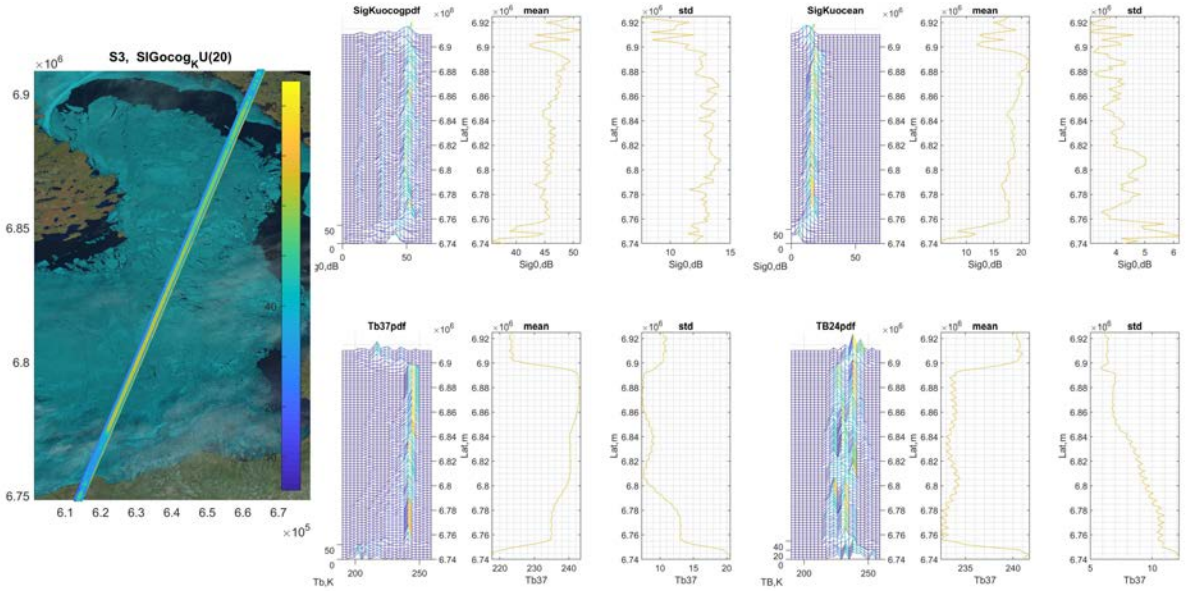

Figure 3.9. Sentinel-3A along-track winter histograms of backscatter, Tb 24 GHz and Tb 37 GHz for: (a) Great Bear Lake and (b) Great Slave Lake. The mean and the standard deviation are calculated from a 1-km window for all winter months (2016-2020). The mean value can be used for assessing spatial variability, while the standard deviation better demonstrates the level of temporal variability at a given latitude.

It appears that for Great Slave Lake the degree of ice fracturing and the location of deformation features (cracks and pressure ridges) significantly vary from year to year, and multi-annual statistics made the interpretation of results difficult (Figure 3.10). This is the reason as to why we limited the time period to a single winter (2019-2020) for which a Sentinel-1 SAR image showing the location of fractured areas was available and the fractured area was sufficiently large.

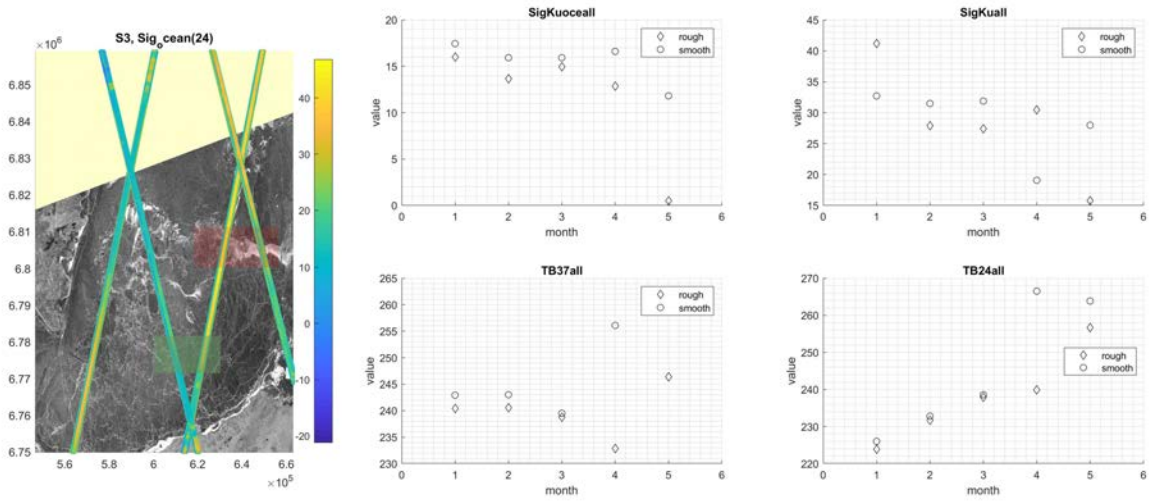

Figure 3.10. Impact of ice cover structure on Sentinel-3A measurements over the Great Slave Lake ice. Values represent a monthly mode estimated for winter 2020 within rough (red box) and smooth (green box) areas defined using Sentinel-1 SAR March 2020 image.

The altimetric radar observations are consistent with the ice characteristics expected for fractured areas: thicker and rougher ice resulting in lower Sig0 values. The presence of pressure ridges does not significantly affect the Tb 24 GHz values until April. In April, a radiative/thermal metamorphosis of snow/ice starts and changes Tb 24 GHz difference (dTb24) between rough and smooth ice zones. It is interesting to note that the sign of dTb24 is different for Great Slave Lake (Figure 3.10) and Great Bear Lake (Figure3.11).

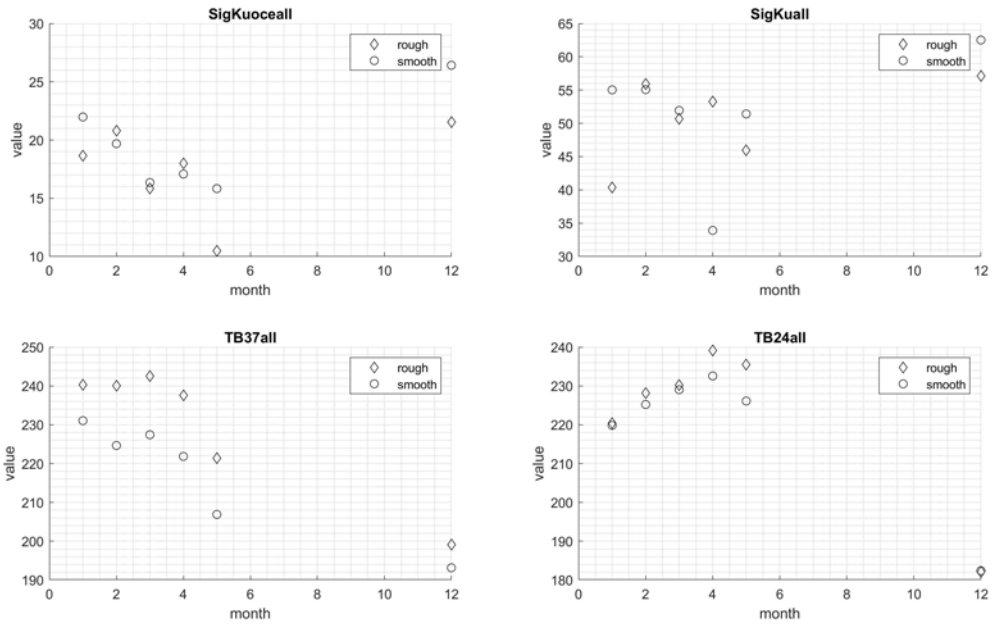

Figure 3.11. Impact of ice structure on Sentinel-3A measurements over Great Bear Lake ice. Values represent the monthly mode estimated for 2016-2020. Rough/smooth areas are defined using spring MODIS quicklooks. The rough area is located between 7355000 m UTM and 7375000 m UTM, the smooth area is located in Dease Arm (Figure 3.2) and bound by 7380000 m UTM - 7410000 m UTM.

A more complex behavior is found for Tb 37 GHz. In agreement with our expectations, the Tb 37 GHz over Great Bear Lake was higher in the rough zone and the temporal variability of this parameter was similar in both areas. For Great Slave Lake, the Tb 37 GHz is slightly higher in the smooth ice zone and rises significantly in April-May compared to the rough ice zone. For instance, based on sensitivity analysis with SMRT, we could suggest that an increase in water content could result in the observed rise of all three parameters (Sig0 Ku, Tb24 and Tb37) in April 2020 in the smooth zone. This increase was not related to meteorological conditions as only the southern part of the lake was affected. Future coupled simulations of CLIMo-SMRT will help to provide a more realistic explanation of the differences in satellite observations over Great Slave Lake.

3.4 Inter-mission comparison

The consistency of satellite measurements from two different altimetric missions (Jason-3 and Sentinel-3A) over the lake ice was verified in a cross-over area of tracks J3_45 and S3A_341 located on Great Slave Lake. Even though the Sig0 of Ice1 (OCOG) retracker is provided for both GDR products, the direct comparison of backscatter measurements is not possible as the Sentinel-3 Sig0 Ice1 retrievals are almost systematically ~35-36 dB higher. Moreover, after 2020, the Sentinel-3A Sig0_OCOG displays a shift (and now better matches the Sig0_Ice1 values of Jason-3). We opted to use the S3 Sig0 retrieved with the Ocean retracker, which is closer to J3 Sig0 Ice1 values. As retracking algorithms are different, the consistency of S-3A and J-3 backscatter measurements can be verified by examination of seasonal variability (Figure 3.12). Caution should be taken, however, regarding the difference in the temporal frequency of satellite observations (10 days vs 27 days). The higher temporal frequency of Jason-3 observations allows for a more precise determination of the ice onset,

which is characterized by very high backscatter values. These dates are missed by Sentinel-3A observations leading to a lower S-3 Sig0 seasonal magnitude.

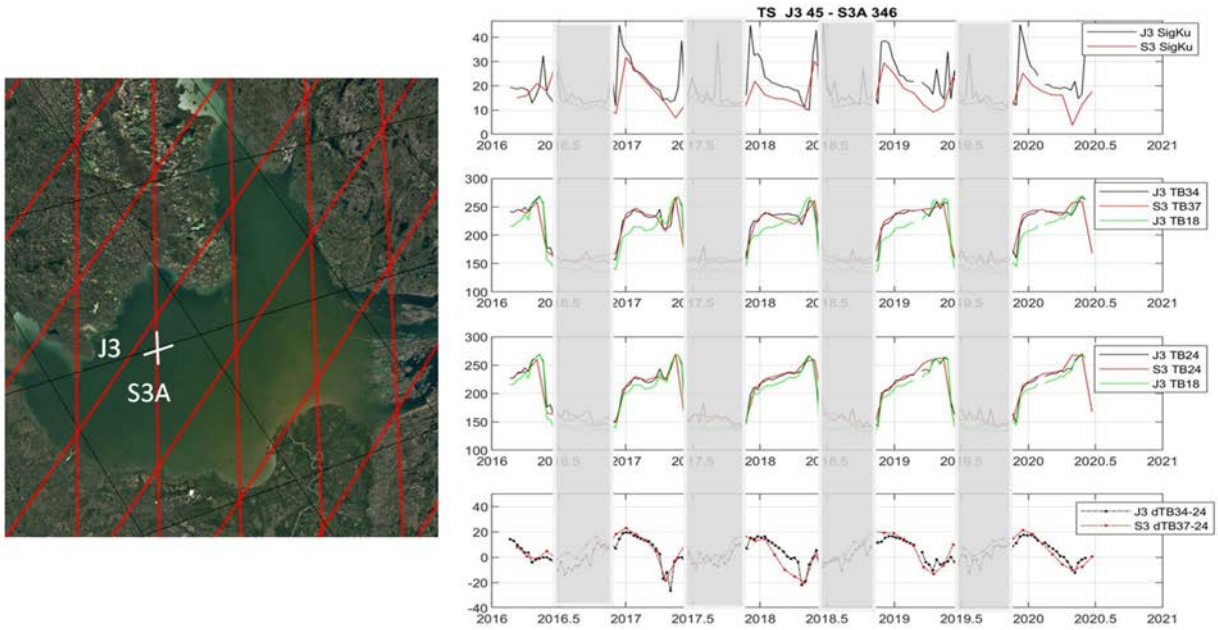

Figure 3.12. Seasonal and interannual variability of Jason-3 and Sentinel-3A backscatter (Ku-band) and brightness temperature (18-37 GHz) measurements in their cross-over over Great Slave Lake.

The inter-satellite bias was evaluated for radar and radiometer measurements considering only months with stable ice/snow cover conditions (January-March) and short (< 4 days) time differences between Jason-3 and Sentinel-3A overpasses. For Tb 34/37 GHz the mean difference is close to 0 and RMSE is 4 °K. The mean Jason-3/Sentinel-3A difference for Tb 24 GHz is -3 °K and RMSE is 3 °K. The difference between Jason-3 Ice1 (OCOG) Sig0 and Sentinel-3A Sig0_ocean is 5 dB with RMSE 6 dB. Our previous studies (e.g. Kang et al., 2014; Duguay et al., in prep.) demonstrated that Tb measurements at 18 GHz are most sensitive to lake ice thickness changes. Knowing that the MWR Sentinel-3 instrument does not provide an 18 GHz band, we plotted the Jason-3 Tb 18 GHz measurements together with Tb 24 GHz and Tb 34/37 GHz measurements to assess their potential co-variability. The seasonal variability and values of Tb 18 GHz are much closer to that of Tb 24 GHz. The average difference between Jason-3 Tb 18 GHz and Sentinel-3A Tb 24 GHz for dates close in time is -11.5 °K and RMSE is 12 °K. Using Jason-3 Tb 18 GHz and Sentinel-3A Tb 24 GHz anomalies, the mean difference is 0.8 °K and RMSE is 4 °K. This proves the good potential of Tb 24 GHz frequency for ice thickness estimation from Sentinel-3A in the absence of an 18 GHz channel.

3.5 Analysis of waveforms

Waveforms (WF) integrate information from different ice layers and surrounding areas, and interpretation of spatio-temporal changes of their shape is not a trivial task. We focused our attention on the evolution of the waveform leading edge and main peak. Temporal analysis of WF acquired over lake ice at the same location reveals a progressive decrease in WF peak power as the ice grows (Figure 3.13) and much lower variability in the far trailing edge. This evolution was observed in Jason-2 Ku-band WF (conventional altimeter) as well as in Sentinel-3 Ku-band WF (SAR altimeter). A similar situation was found for river ice (Zakharova et al., 2020). Considering that the Ku-band radar signal penetrates into lake ice and the main WF peak is related to the power portion backscattered from ice/water interface, the temporal decrease of main peak power corresponds well to the increase of the volumetric scattering

with ice thickening.

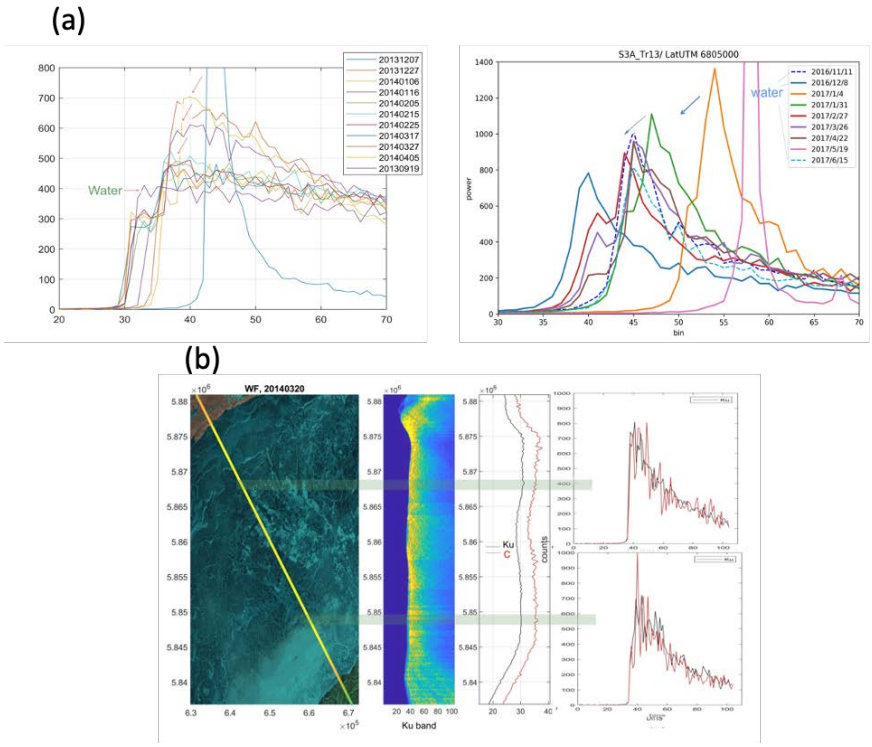

Figure 3.13. Evolution of waveforms at Ku-band over (a) Great Slave Lake for different dates in winter 2013-2014 5 (Jason-2) and winter 2016-2017 (Sentinel-3A) and (b) Lake Baikal snow-free ice (top right graph) and snow-covered ice (bottom right graph) on 20 March 2014. Waveforms in black are Ku-band and red are C-band.

Mercier et al. (2014) and Beckers et al. (2017) noted the presence of an intermediate peak on the leading edge of the radar echo, which is interpreted as the scattering from the air/ice or air/snow interface (ice surface), while the main peak is considered to come from the ice/water interface (ice bottom). In most radar waveforms over the Great Slave Lake, we also detect this intermediate peak on the leading edge. However, on Lake Baikal ice, many return echoes are mono-peaky (Figure 3.13 b). The mono-peaky waveforms can be found in areas of clear (congelation) ice with the absence of an overlying snow cover.

4. SUMMARY AND NEXT STEPS

In this document, we reported on progress and findings from WP 200 (Forward modelling of backscatter and brightness temperature using the SMRT model) and 310 (Analysis of altimetry and radiometer data over lakes).

For WP 200, progress has been made on several fronts: 1) adaptation of the SMRT model and completion of a set of simulations to examine the sensitivity of brightness temperature and backscatter to ice thickness, and the influence of various ice (snow ice, bubbles, roughness at ice-water interface) and snow (depth, wetness) properties affecting microwave signals, which could be considered as potential sources of uncertainty in ice thickness retrievals from altimeter missions; 2) preliminary simulations of waveforms (low resolution mode) with a new altimetry module recently added to SMRT; and 3) coupling of the Canadian Lake Ice Model (CLIMo) with SMRT.

Results from SMRT simulations in standalone mode (i.e. not coupled with CLIMo) indicate that:

- Brightness temperature (Tb) increases with ice thickness, and the sensitivity highly depends on frequency. The sensitivity is greater at lower (18.7 and 23.8 GHz) than higher frequencies (34.0 and 36.5 GHz). Backscatter over clear ice (with or without snow) is sensitive to ice thickness only (clearly) at Ku-band.

- The presence of dry snow on the ice surface can result in a large increase of Tb. The main role of snow is due to impedance matching and the most critical parameter is therefore the density, through its control on snow permittivity.
- Tb decreases with bubble size in the snow ice layer and the effect is much more significant at the higher frequencies. While this affects the Tb = f(ice thickness) relation, the perturbing effect is more marked at 34.0 and 36.5 GHz. Bubble size also impacts the sensitivity of backscatter to ice thickness. The relation between backscatter ice thickness becomes more and more sensitive as the bubble size increases at Ku band. Snow ice is contributing to the Ku-band signal by attenuating the backscatter coming from the bottom ice-water interface.
- The roughness at the ice-water interface has a large impact on Tb. The effect of roughness is large and is more visible at the lower frequencies due to larger penetration depths than at higher frequencies. This value is critical to determine the Tb = f(ice thickness) relation. It must be known, and the higher frequencies are not useful for this. The ice-water interface is the main source of backscatter and the dependency to roughness is significant at Ku-band and lower frequencies. C and S-band are even more sensitive to the roughness of the bottom interface, and may then serve to retrieve this information, as these bands have little dependency on ice thickness.
- The presence of liquid water in snow has a large impact on Tb. When snow is wet, there is an increase in signal absorption. As a result, the signal coming from below tis layer is unable to “escape” the ice. The sensitivity to ice thickness and any other property of the ice vanishes under such condition.

Several questions were investigated under WP 310. Results can be summarized as follows:

- Land can contaminate backscatter and Tb measurements to various degrees. The impact of land on backscatter gradually decreased, in general, to a distance of 1.5 to 4 km from the coast at Ku and C-band. For cases where there is a high contrast between land and ice, the land effect can be negligible on Tb. In cases of low land/ice contrast, Tb measurements at 37 GHz are not affected by land at a 2-10-km distances from the coast. At 24 GHz, the land effect on Tb measurements over lake ice fully disappears at 18-20 km (high land/ice contrast) and 14-15 km from the coast (low land/ice contrast).
- Snow depth of the order of 20-80 cm can result in a 2-3 dB decrease in backscatter compared to snow-free conditions at both Ku and C-band. This was demonstrated using Jason-2 measurements over Lake Baikal. The effect of snow on the radiometric measurements differs depending on frequency and time during the ice growth season. Snow increases Tb by 4°K at 34 GHz and 6°K at 18 GHz and 24 GHz early in season. The difference in Tb between snow-covered and snow-free clear ice disappears at 18 GHz later in the season and reduces by 2-3°K at 24 and 37 GHz.
- The impact of ice structure is observed in backscatter measurements. Thicker and rougher ice result in lower backscatter values. The presence of pressure ridges does not impact as significantly Tb measurements.
- The inter-comparison of radar and radiometer measurements of Jason-3 and Sentinel-3 missions reveal that backscatter values can be significantly different depending on the retracker used (Ice1 OCOG vs Ocean). Large differences also exist for Tb for some frequencies. However, the mean difference was found to be only 0.8 °K and RMSE 4 °K between Jason-3 Tb (18 GHz) and Sentinel-3A Tb (24 GHz), which points to the potential of Sentinel-3 24 GHz for estimating ice thickness.
- The spatio-temporal variability of Jason-2 waveforms can be exploited to derive ice thickness. When ice is overlain by a snow cover (e.g. Great Slave Lake), the presence of an intermediate peak on the leading edge of the radar echo can interpreted as the scattering from the air/ice or air/snow interface, while the main peak is considered to come from the ice/water interface. However, when ice sections of lakes are snow-free (e.g Lake Baikal) return echoes are mono-peaky. In such case, retrieval of ice thickness may not be possible based on the analysis of waveforms.

Finally, it should be noted that simulations and interpretation of results obtained with SMRT (WP 200) were done independently from the interpretation of backscatter and Tb measurements from altimeter missions (WP 310). The two WPs were purposely run in parallel. Results from both WPs show some general agreements regarding the sensitivity of Tb and backscatter to lake ice thickness and other properties, including snow characteristics, but also some discrepancies. Therefore, work to be conducted under WP 320 will involve comparison of SMRT simulations (WP 200) with altimetry and radiometer observations (WP 310) over the same lakes. This will help to elucidate some of the discrepancies between model output and observations. For this purpose, coupled CLIMo-SMRT simulations will be performed as to provide a more realistic representation of ice and snow properties than what is possible with SMRT in standalone mode (e.g. temperature profile in ice and snow, snow ice formation). For these simulations, focus will be on relatively homogeneous areas of lakes since SMRT cannot represent 3-D features such as pressure ridges. Results from WP 320 and WP 400 (Conclusions and recommendations for future work (roadmap) will be covered in the Final Report.

5. REFERENCES

Beckers, J.F., J.A. Casey, and C. Haas, 2017. Retrievals of lake ice thickness from Great Slave Lake and Great Bear Lake using CryoSat-2. *IEEE Transactions on Geoscience and Remote Sensing*, 55(7): 3708-3720, doi: 10.1109/TGRS.2017.2677583.

Brown, L.C. and C.R. Duguay, 2011. A comparison of simulated and measured lake ice thickness using a Shallow Water Ice Profiler. *Hydrological Processes*, 25: 2932-2941, doi: 10.1002/hyp.8087.

Duguay, C.R., G.M. Flato, M.O. Jeffries, P. Ménard, K. Morris, and W.R. Rouse, 2003. Ice cover variability on shallow lakes at high latitudes: Model simulations and observations. *Hydrological Processes*, 17: 3465-3483.

Duguay, C.R., E.A. Zakharova, A.V. Kouraev, H. Kheyrollah Pour, and J. Murfitt, in prep. Estimation of lake ice thickness from Jason-2 radar altimetry and passive microwave radiometry.

ESA, 2012. Report for mission selection: $CoReH_2O$, ESA SP-1324/2 (3 volume series), European Space Agency, Noordwijk, The Netherlands.

Fung, A.K., Z. Li, and K.S. Chen, 1992. Backscattering from a randomly rough dielectric surface. *IEEE Transactions on Geoscience and Remote Sensing*, 30(2): 356-369. doi: http://dx.doi.org/10.1109/36.134085.

Kang, K.-K., C.R. Duguay, J. Lemmetyinen, and Y. Gel, 2014. Estimation of ice thickness on large northern lakes from AMSR-E brightness temperature measurements. *Remote Sensing of Environment*, 150: 1-19, http://dx.doi.org/10.1016/j.rse.2014.04.016.

Kouraev, A.V., Shimaraev, M.N., Buharizin, P.I. et al, 2008. Ice and snow cover of continental water bodies from simultaneous radar altimetry and radiometry observations. Surveys of Geophysics, 29: 271-295, https://doi.org/10.1007/s10712-008-9042-2.

Mercier F., J., Tournade, A. Kouraev, O. Gaquiere, and E. Leguay, 2011. Iceberg detection and continental lake ice thickness estimation using altimeter waveforms. *2nd SARAL/ALTIKA Science Workshop*, Ahmedabad, March 15-17.

Picard, G., M. Sandells, and H. Löwe, 2018. SMRT: An active / passive microwave radiative transfer model for snow with multiple microstructure and scattering formulations (v1.0). *Geoscientific Model Development*, 11: 2763-2788, doi:10.5194/gmd-11-2763-2018.

Sihvola, A., 1999. Electromagnetic mixing formulas and applications, Institution of Engineering & T, 296 pp., ISBN: 0852967721.

Vargel, C., A. Royer, O. St-Jean-Rondeau, G. Picard, A. Roy, V. Sasseville, A. Langlois, 2020. Arctic and subarctic snow microstructure analysis for microwave brightness temperature simulations, *Remote Sensing of Environment*, 242, 111754, https://doi.org/10.1016/j.rse.2020.111754.

Zakharova, E., S. Agafonova, C. Duguay C., N. Frolova, and A. Kouraev, 2020. River ice phenology and thickness from satellite altimetry. Potential for ice bridge road operation. *The Cryosphere Discussions*, doi: 10.5194/tc-2020-325. In review for *The Cryosphere*.

Appendix

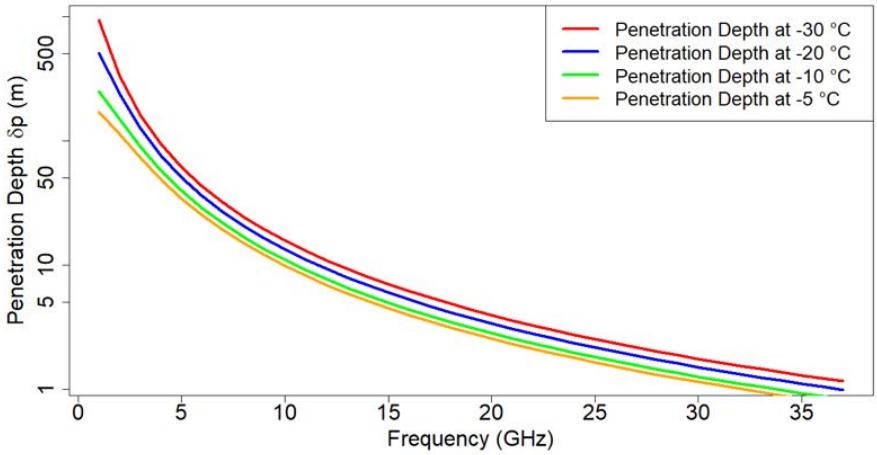

Figure A1. Penetration depths in clear ice with no overlying snow as a function of frequency for different ice temperatures.

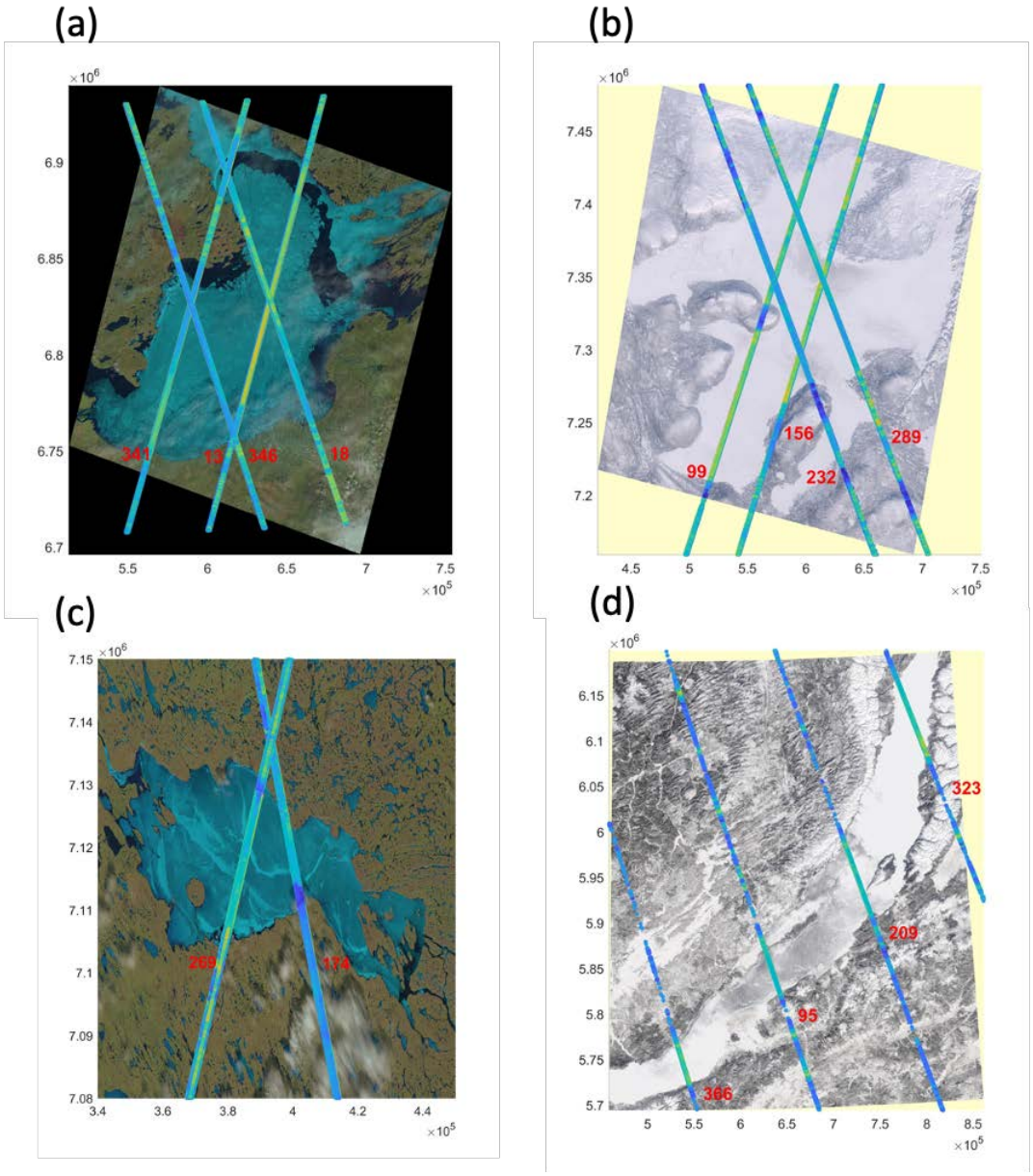

Figure A2. Location of the Sentinel-3A tracks used for construction of histograms presented on figures 3.4-3.8 for Great Slave (a), Great Bear (b), Baker (c) and Baikal (d) lakes. Maps coordinates are given in UTM meters.